Finite difference schemes with transferable interfaces for parabolic problems

Sofia Eriksson and Jan Nordström

Eriksson, S., Nordström, J., (2018), Finite difference schemes with transferable interfaces for parabolic problems, *Journal of Computational Physics*, 375, 935-949.
https://doi.org/10.1016/j.jcp.2018.08.051

Finite difference schemes with transferable interfaces for parabolic problems

Sofia Eriksson Jan Nordström

Abstract

We derive a method to locally change the order of accuracy of finite difference schemes that approximate the second derivative. The derivation is based on summation-by-parts operators, which are connected at interfaces using penalty terms. At such interfaces, the numerical solution has a double representation, with one representation in each domain. We merge this double representation into a single one, yielding a new scheme with unique solution values in all grid points. The resulting scheme is proven to be stable, accurate and dual consistent.

Keywords: Finite difference methods, summation-by-parts, high order accuracy, dual consistency, superconvergence, interfaces

1 Introduction

We consider summation-by-parts (SBP) finite difference methods with weakly imposed boundary and interface conditions using simultaneous approximation terms (SAT). The main advantages of the SBP-SAT technique are high accuracy, computational efficiency and provable time-stability. For a background on the SBP-SAT technique, see [16, 5].

At SAT interfaces, the numerical solution has a double, collocated representation, with one solution value belonging to each side of the interface [2, 12]. The two values are allowed to deviate slightly from each other. SAT interfaces are useful when generating grids for complex geometries or – as in our case – when changing the properties of the scheme in parts of the computational domain. However, if the interface must be moved during the computation, e.g. to keep track of a moving shock, it is more convenient that the solution is single-valued at each grid point.

Our approach to derive such single-valued interfaces, is to use the double-valued SAT interface treatment as a starting point, merge the double representation at the interface into a single one and obtain a new set of operators. This was done in [4] for hyperbolic problems and here we extend that methodology to parabolic problems. These new operators will make it easier to switch the order of accuracy locally, in for example Navier–Stokes calculations, when shock capturing or sharp gradient resolution for course meshes is required.

The paper is organized as follows: In Section 2, we present our parabolic model problem; the heat equation with an artificial interface. This problem is discretized in

space in Section 3, using a standard SAT interface. Next, in Section 4, we merge the double representation at the SAT interface into a single representation, giving us the new scheme, which is shown to be stable, accurate and dual consistent in Section 5. The theoretical results are confirmed by numerical experiments in Section 6, and a summary is given in Section 7, concluding the paper.

2 The model problem

To introduce our technique, we consider the one-dimensional scalar heat equation, with an interface at an interior point $\hat{x}$, as

$$\begin{aligned} u_t^{\mathrm{L}} &= \varepsilon u_{xx}^{\mathrm{L}}, & x \in \Omega_{\mathrm{L}} = [0, \hat{x}], \\ u_t^{\mathrm{R}} &= \varepsilon u_{xx}^{\mathrm{R}}, & x \in \Omega_{\mathrm{R}} = [\hat{x}, 1], \end{aligned} \tag{1}$$

which is complemented with an interface condition at $x = \hat{x}$, boundary conditions at $x = 0, 1$ and initial data at $t = 0$.

2.1 Well-posedness

The problem (1) is well-posed if it has a unique solution and if it is bounded by data, see [13, 7]. To show boundedness, we use the energy method.

We multiply the two equations in (1) by $u^{\mathrm{L,R}}$ and integrate over their respective domains. Using integration by parts, and thereafter adding the two results, yields

$$\frac{\mathrm{d}}{\mathrm{d}t} \left(\|u^{\mathrm{L}}\|^2 + \|u^{\mathrm{R}}\|^2 \right) + 2\varepsilon \left(\|u_x^{\mathrm{L}}\|^2 + \|u_x^{\mathrm{R}}\|^2 \right) = \mathrm{BT} + \mathrm{IT} \tag{2}$$

where $\|u\|^2 = \int_0^1 u^2 \, \mathrm{d}x$. To make the presentation clear, we ignore the boundary terms $\mathrm{BT} = -2\varepsilon u^{\mathrm{L}} u_x^{\mathrm{L}}\big|_0 + 2\varepsilon u^{\mathrm{R}} u_x^{\mathrm{R}}\big|_1$ and focus on the interface terms $\mathrm{IT} = 2\varepsilon \left(u^{\mathrm{L}} u_x^{\mathrm{L}} - u^{\mathrm{R}} u_x^{\mathrm{R}} \right)\big|_{\hat{x}}$. We need $\mathrm{IT} \leq 0$ to bound the growth of the solution. Here we aim for an artificial interface and first demand continuity, that is $u^{\mathrm{L}}|_{\hat{x}} = u^{\mathrm{R}}|_{\hat{x}}$. To achieve $\mathrm{IT} = 0$, we also need $u_x^{\mathrm{L}}|_{\hat{x}} = u_x^{\mathrm{R}}|_{\hat{x}}$. Hence, the interface conditions related to (1) are

$$u^{\mathrm{L}}(\hat{x}, t) = u^{\mathrm{R}}(\hat{x}, t), \qquad u_x^{\mathrm{L}}(\hat{x}, t) = u_x^{\mathrm{R}}(\hat{x}, t). \tag{3}$$

3 Discretization

We use the method of lines and discretize the spatial domain $\Omega = [0, 1]$ using $N + 1$ equidistant grid points $x_j = jh$, where $h = 1/N$ is the grid spacing and $j = 0, 1, \ldots, N$. Next, we introduce a numerical interface at $\hat{x}$, where $\hat{x}$ coincides with some interior grid point $x_{\hat{\imath}}$. This gives us $N_{\mathrm{L}} + 1$ grid points in Ω_{L} and $N_{\mathrm{R}} + 1$ grid points in Ω_{R}, where $N_{\mathrm{L}} = \hat{\imath}$ and $N_{\mathrm{R}} = N - \hat{\imath}$.

3.1 The SBP operators

Let the vector $\mathbf{f} = [\mathbf{f}_0, \mathbf{f}_1 \ldots, \mathbf{f}_N]^{\mathsf{T}}$ be a discrete representation of the continuous function $f(x, t)$, such that $\mathbf{f}_j(t) = f(x_j, t)$. A discrete differential operator D_1, that approximates

$\partial/\partial x$ such that $(D_1\mathbf{f})_j(t) \approx f_x(x_j,t)$, is an SBP-operator if it can be factorized as

$$D_1 = P^{-1}Q, \qquad P = P^\mathsf{T} > 0, \qquad Q + Q^\mathsf{T} = E_N - E_0, \tag{4}$$

where $E_0 = \mathbf{e}_0\mathbf{e}_0^\mathsf{T}$, $E_N = \mathbf{e}_N\mathbf{e}_N^\mathsf{T}$, $\mathbf{e}_0 = [1,0,\ldots,0]^\mathsf{T}$ and $\mathbf{e}_N = [0,\ldots,0,1]^\mathsf{T}$. Later we use that P is diagonal, and hence D_1 consists of central, $2p$-order accurate finite difference stencils in the interior and one-sided, p-order accurate stencils at the boundaries [9, 14, 10].

To approximate the second derivative operator $\partial^2/\partial x^2$ we use the operator D_2, and – in addition to consistency – demand that it fulfills the SBP properties

$$D_2 = P^{-1}\left(-A + \mathbf{e}_N\mathbf{d}_N^\mathsf{T} - \mathbf{e}_0\mathbf{d}_0^\mathsf{T}\right), \qquad A = A^\mathsf{T} \geq 0, \tag{5}$$

where $\mathbf{d}_0^\mathsf{T}\mathbf{f} \approx f_x(0,t)$ and $\mathbf{d}_N^\mathsf{T}\mathbf{f} \approx f_x(1,t)$. For stability $A + A^\mathsf{T} \geq 0$ suffice, but for dual consistency we need A to be symmetric [3]. The notations $>$ and $\geq$ refer to positive definite and positive semi-definite matrices, respectively, and the vectors $\mathbf{e}_0$, $\mathbf{e}_N$, $\mathbf{d}_0$ and $\mathbf{d}_N$ have dimensions $(N+1)\times 1$.

The form of D_2 in (5) is consistent with the wide-stencil case where $D_2^\mathrm{w} \equiv D_1^2$, since we, using the properties in (4), can write $D_2^\mathrm{w} = P^{-1}(-D_1^\mathsf{T}PD_1 + \mathbf{e}_N\mathbf{e}_N^\mathsf{T}D_1 - \mathbf{e}_0\mathbf{e}_0^\mathsf{T}D_1)$. Identifying the terms in (5), we see that in the wide-stencil case they are

$$A^\mathrm{w} = D_1^\mathsf{T}PD_1, \qquad \mathbf{d}_0^\mathrm{w} = D_1^\mathsf{T}\mathbf{e}_0, \qquad \mathbf{d}_N^\mathrm{w} = D_1^\mathsf{T}\mathbf{e}_N.$$

In the general case (including narrow-stencil operators) we let

$$A = S^\mathsf{T}MS, \qquad \mathbf{d}_0 = S^\mathsf{T}\mathbf{e}_0, \qquad \mathbf{d}_N = S^\mathsf{T}\mathbf{e}_N, \tag{6}$$

where the first and last row of the matrix S are consistent difference stencils [2]. The interior of S is not uniquely defined and neither is the matrix M, but they can be chosen such that $M > 0$. The operators used in this work can all be found in [11].

3.2 The SAT interface treatment

We return to the two coupled heat equations in (1). Let $\mathbf{u}_{\mathrm{L,R}}$ denote the semi-discrete approximations of $u^{\mathrm{L,R}}$. We approximate $\partial^2/\partial x^2$ by $D_{2,\mathrm{L}}$ and $D_{2,\mathrm{R}}$ in the two domains, respectively, both fulfilling the properties in (5). However, since we ignore the outer boundaries, we simplify and write

$$D_{2,\mathrm{L}} = P_\mathrm{L}^{-1}\left(-A_\mathrm{L} + \mathbf{e}_{N,\mathrm{L}}\mathbf{d}_{N,\mathrm{L}}^\mathsf{T}\right), \qquad D_{2,\mathrm{R}} = P_\mathrm{R}^{-1}\left(-A_\mathrm{R} - \mathbf{e}_{0,\mathrm{R}}\mathbf{d}_{0,\mathrm{R}}^\mathsf{T}\right), \tag{7}$$

for ease of presentation. The vectors $\mathbf{u}_\mathrm{L}$, $\mathbf{e}_{N,\mathrm{L}}$ and $\mathbf{d}_{N,\mathrm{L}}$ have dimensions $(N_\mathrm{L}+1)\times 1$ and the vectors $\mathbf{u}_\mathrm{R}$, $\mathbf{e}_{0,\mathrm{R}}$ and $\mathbf{d}_{0,\mathrm{R}}$ have dimensions $(N_\mathrm{R}+1)\times 1$, where $N_\mathrm{L} + N_\mathrm{R} = N$.

The two interface conditions from (3) are imposed using penalty terms proportional to $\mathbf{e}_{N,\mathrm{L}}^\mathsf{T}\mathbf{u}_\mathrm{L} - \mathbf{e}_{0,\mathrm{R}}^\mathsf{T}\mathbf{u}_\mathrm{R}$, which approximates $u^\mathrm{L}(\hat{x},t) - u^\mathrm{R}(\hat{x},t)$, and to $\mathbf{d}_{N,\mathrm{L}}^\mathsf{T}\mathbf{u}_\mathrm{L} - \mathbf{d}_{0,\mathrm{R}}^\mathsf{T}\mathbf{u}_\mathrm{R}$, which approximates $u_x^\mathrm{L}(\hat{x},t) - u_x^\mathrm{R}(\hat{x},t)$. The spatial discretization of (1) is thus given by

$$\begin{aligned}
\frac{\mathrm{d}}{\mathrm{d}t}\mathbf{u}_\mathrm{L} &= \varepsilon D_{2,\mathrm{L}}\mathbf{u}_\mathrm{L} + P_\mathrm{L}^{-1}(\sigma_\mathrm{L}^1\mathbf{e}_{N,\mathrm{L}} + \sigma_\mathrm{L}^2\mathbf{d}_{N,\mathrm{L}})(\mathbf{e}_{N,\mathrm{L}}^\mathsf{T}\mathbf{u}_\mathrm{L} - \mathbf{e}_{0,\mathrm{R}}^\mathsf{T}\mathbf{u}_\mathrm{R}) \\
&\quad + P_\mathrm{L}^{-1}(\sigma_\mathrm{L}^3\mathbf{e}_{N,\mathrm{L}} + \sigma_\mathrm{L}^4\mathbf{d}_{N,\mathrm{L}})(\mathbf{d}_{N,\mathrm{L}}^\mathsf{T}\mathbf{u}_\mathrm{L} - \mathbf{d}_{0,\mathrm{R}}^\mathsf{T}\mathbf{u}_\mathrm{R}), \\
\frac{\mathrm{d}}{\mathrm{d}t}\mathbf{u}_\mathrm{R} &= \varepsilon D_{2,\mathrm{R}}\mathbf{u}_\mathrm{R} + P_\mathrm{R}^{-1}(\sigma_\mathrm{R}^1\mathbf{e}_{0,\mathrm{R}} + \sigma_\mathrm{R}^2\mathbf{d}_{0,\mathrm{R}})(\mathbf{e}_{0,\mathrm{R}}^\mathsf{T}\mathbf{u}_\mathrm{R} - \mathbf{e}_{N,\mathrm{L}}^\mathsf{T}\mathbf{u}_\mathrm{L}) \\
&\quad + P_\mathrm{R}^{-1}(\sigma_\mathrm{R}^3\mathbf{e}_{0,\mathrm{R}} + \sigma_\mathrm{R}^4\mathbf{d}_{0,\mathrm{R}})(\mathbf{d}_{0,\mathrm{R}}^\mathsf{T}\mathbf{u}_\mathrm{R} - \mathbf{d}_{N,\mathrm{L}}^\mathsf{T}\mathbf{u}_\mathrm{L}),
\end{aligned} \tag{8}$$

where the penalty parameters $\sigma_{\mathrm{L}}^{1,2,3,4}$ and $\sigma_{\mathrm{R}}^{1,2,3,4}$ will be chosen such that the scheme (8) becomes accurate, stable and dual consistent.

Remark 3.1. Choosing $\sigma_{\mathrm{L,R}}^{4} \neq 0$ affects the spectrum of the final operators strongly, easily making the resulting new scheme very stiff, but for the sake of generality we keep these parameters in the derivations.

3.3 Dual consistency

We will choose the penalty parameters $\sigma_{\mathrm{L,R}}^{1,2,3,4}$ above such that the scheme becomes dual consistent [8]. We start by rewriting (8) more compactly, as

$$\frac{\mathrm{d}}{\mathrm{d}t}\vec{\mathbf{u}} = L\vec{\mathbf{u}}, \tag{9}$$

where

$$L = \varepsilon \begin{bmatrix} D_{2,\mathrm{L}} & 0 \\ 0 & D_{2,\mathrm{R}} \end{bmatrix} + \overline{P}^{-1} \begin{bmatrix} \sigma_{\mathrm{L}}^{1}\mathbf{e}_{N,\mathrm{L}} + \sigma_{\mathrm{L}}^{2}\mathbf{d}_{N,\mathrm{L}} \\ -\sigma_{\mathrm{R}}^{1}\mathbf{e}_{0,\mathrm{R}} - \sigma_{\mathrm{R}}^{2}\mathbf{d}_{0,\mathrm{R}} \end{bmatrix} \vec{\mathbf{e}}^{\mathsf{T}} + \overline{P}^{-1} \begin{bmatrix} \sigma_{\mathrm{L}}^{3}\mathbf{e}_{N,\mathrm{L}} + \sigma_{\mathrm{L}}^{4}\mathbf{d}_{N,\mathrm{L}} \\ -\sigma_{\mathrm{R}}^{3}\mathbf{e}_{0,\mathrm{R}} - \sigma_{\mathrm{R}}^{4}\mathbf{d}_{0,\mathrm{R}} \end{bmatrix} \vec{\mathbf{d}}^{\mathsf{T}}$$

and

$$\vec{\mathbf{u}} = \begin{bmatrix} \mathbf{u}_{\mathrm{L}} \\ \mathbf{u}_{\mathrm{R}} \end{bmatrix}, \qquad \overline{P} = \begin{bmatrix} P_{\mathrm{L}} & 0 \\ 0 & P_{\mathrm{R}} \end{bmatrix}, \qquad \vec{\mathbf{e}} = \begin{bmatrix} \mathbf{e}_{N,\mathrm{L}} \\ -\mathbf{e}_{0,\mathrm{R}} \end{bmatrix}, \qquad \vec{\mathbf{d}} = \begin{bmatrix} \mathbf{d}_{N,\mathrm{L}} \\ -\mathbf{d}_{0,\mathrm{R}} \end{bmatrix}. \tag{10}$$

Note that the differences between the double interface representations can be expressed as $\vec{\mathbf{e}}^{\mathsf{T}}\vec{\mathbf{u}} = \mathbf{e}_{N,\mathrm{L}}^{\mathsf{T}}\mathbf{u}_{\mathrm{L}} - \mathbf{e}_{0,\mathrm{R}}^{\mathsf{T}}\mathbf{u}_{\mathrm{R}}$ and $\vec{\mathbf{d}}^{\mathsf{T}}\vec{\mathbf{u}} = \mathbf{d}_{N,\mathrm{L}}^{\mathsf{T}}\mathbf{u}_{\mathrm{L}} - \mathbf{d}_{0,\mathrm{R}}^{\mathsf{T}}\mathbf{u}_{\mathrm{R}}$. The vectors $\vec{\mathbf{u}}$, $\vec{\mathbf{e}}$ and $\vec{\mathbf{d}}$ have dimensions $(N+2)\times 1$, and L and $\overline{P}$ are $(N+2)\times(N+2)$-matrices.

Now consider a continuous equation $u_t = \mathcal{L}u$, where $\mathcal{L}$ is a linear, spatial differential operator. Its so called dual (or adjoint) equation is $-v_t = \mathcal{L}^* v$, where the dual operator $\mathcal{L}^*$ is specified by $\langle v, \mathcal{L}u\rangle = \langle \mathcal{L}^* v, u\rangle$ and where the inner product is $\langle v, u\rangle \equiv \int_0^1 vu\,\mathrm{d}x$. For a scheme $\vec{\mathbf{u}}_t = L\vec{\mathbf{u}}$ to be a dual consistent approximation of $u_t = \mathcal{L}u$, we need L^*, where L^* is the *discrete* dual operator, to be a consistent approximation of $\mathcal{L}^*$. Using the relation $\langle \vec{\mathbf{v}}, L\vec{\mathbf{u}}\rangle_{\overline{P}} = \langle L^*\vec{\mathbf{v}}, \vec{\mathbf{u}}\rangle_{\overline{P}}$, with $\langle \vec{\mathbf{v}}, \vec{\mathbf{u}}\rangle_{\overline{P}} \equiv \vec{\mathbf{v}}^{\mathsf{T}}\overline{P}\vec{\mathbf{u}}$, one finds that the discrete dual operator is $L^* \equiv \overline{P}^{-1}L^{\mathsf{T}}\overline{P}$ [1].

In our case we consider $u_t = \varepsilon u_{xx}$, thus $\mathcal{L} = \varepsilon\partial^2/\partial x^2$. Next, we note that $\mathcal{L}$ is a self-adjoint operator, since $\mathcal{L}^* = \varepsilon\partial^2/\partial x^2$. This means that for (9) to be dual consistent, not only L but also L^* must be a consistent numerical approximation of $\mathcal{L} = \mathcal{L}^* = \varepsilon\partial^2/\partial x^2$.

We compute the discrete dual operator $L^* = \overline{P}^{-1}L^{\mathsf{T}}\overline{P}$. Using the SBP-properties (5) (here we need A_{L}, A_{R} to be symmetric) we obtain

$$\begin{aligned} L^* = \varepsilon \begin{bmatrix} D_{2,\mathrm{L}} & 0 \\ 0 & D_{2,\mathrm{R}} \end{bmatrix} &+ \overline{P}^{-1} \begin{bmatrix} (\sigma_{\mathrm{L}}^{1}\mathbf{e}_{N,\mathrm{L}} + (\sigma_{\mathrm{L}}^{3}+\varepsilon)\mathbf{d}_{N,\mathrm{L}})\mathbf{e}_{N,\mathrm{L}}^{\mathsf{T}} & -(\sigma_{\mathrm{R}}^{1}\mathbf{e}_{N,\mathrm{L}} + \sigma_{\mathrm{R}}^{3}\mathbf{d}_{N,\mathrm{L}})\mathbf{e}_{0,\mathrm{R}}^{\mathsf{T}} \\ -(\sigma_{\mathrm{L}}^{1}\mathbf{e}_{0,\mathrm{R}} + \sigma_{\mathrm{L}}^{3}\mathbf{d}_{0,\mathrm{R}})\mathbf{e}_{N,\mathrm{L}}^{\mathsf{T}} & (\sigma_{\mathrm{R}}^{1}\mathbf{e}_{0,\mathrm{R}} + (\sigma_{\mathrm{R}}^{3}-\varepsilon)\mathbf{d}_{0,\mathrm{R}})\mathbf{e}_{0,\mathrm{R}}^{\mathsf{T}} \end{bmatrix} \\ &+ \overline{P}^{-1} \begin{bmatrix} ((\sigma_{\mathrm{L}}^{2}-\varepsilon)\mathbf{e}_{N,\mathrm{L}} + \sigma_{\mathrm{L}}^{4}\mathbf{d}_{N,\mathrm{L}})\mathbf{d}_{N,\mathrm{L}}^{\mathsf{T}} & -(\sigma_{\mathrm{R}}^{2}\mathbf{e}_{N,\mathrm{L}} + \sigma_{\mathrm{R}}^{4}\mathbf{d}_{N,\mathrm{L}})\mathbf{d}_{0,\mathrm{R}}^{\mathsf{T}} \\ -(\sigma_{\mathrm{L}}^{2}\mathbf{e}_{0,\mathrm{R}} + \sigma_{\mathrm{L}}^{4}\mathbf{d}_{0,\mathrm{R}})\mathbf{d}_{N,\mathrm{L}}^{\mathsf{T}} & ((\sigma_{\mathrm{R}}^{2}+\varepsilon)\mathbf{e}_{0,\mathrm{R}} + \sigma_{\mathrm{R}}^{4}\mathbf{d}_{0,\mathrm{R}})\mathbf{d}_{0,\mathrm{R}}^{\mathsf{T}} \end{bmatrix}. \end{aligned}$$

For L^* to be a consistent approximation of $\mathcal{L}^* = \varepsilon\partial^2/\partial x^2$, it must have the same form as L in (9). To be exact, the penalty portion of L^* must consists of one part proportional to $\vec{\mathbf{e}}$ and one part proportional to $\vec{\mathbf{d}}$. This is only possible if the relations

$$\sigma_{\mathrm{L}}^{1} = \sigma_{\mathrm{R}}^{1}, \qquad \sigma_{\mathrm{L}}^{3} + \varepsilon = \sigma_{\mathrm{R}}^{3}, \qquad \sigma_{\mathrm{L}}^{2} - \varepsilon = \sigma_{\mathrm{R}}^{2}, \qquad \sigma_{\mathrm{L}}^{4} = \sigma_{\mathrm{R}}^{4} \tag{11}$$

hold. The proportionality with $\vec{\mathbf{e}}$ and $\vec{\mathbf{d}}$ is necessary since it means that the coupling conditions $\vec{\mathbf{e}}^{\mathsf{T}}\vec{\mathbf{u}} = \mathbf{e}_{N,\mathrm{L}}^{\mathsf{T}}\mathbf{u}_{\mathrm{L}} - \mathbf{e}_{0,\mathrm{R}}^{\mathsf{T}}\mathbf{u}_{\mathrm{R}} \approx 0$ and $\vec{\mathbf{d}}^{\mathsf{T}}\vec{\mathbf{u}} = \mathbf{d}_{N,\mathrm{L}}^{\mathsf{T}}\mathbf{u}_{\mathrm{L}} - \mathbf{d}_{0,\mathrm{R}}^{\mathsf{T}}\mathbf{u}_{\mathrm{R}} \approx 0$ are imposed. If the penalty part of L^* does not have this form, some other coupling conditions are imposed on the dual problem. The specific choices in (11) leads to

$$L^* = \varepsilon \begin{bmatrix} D_{2,\mathrm{L}} & 0 \\ 0 & D_{2,\mathrm{R}} \end{bmatrix} + \overline{P}^{-1} \begin{bmatrix} \sigma_{\mathrm{R}}^1 \mathbf{e}_{N,\mathrm{L}} + \sigma_{\mathrm{R}}^3 \mathbf{d}_{N,\mathrm{L}} \\ -\sigma_{\mathrm{L}}^1 \mathbf{e}_{0,\mathrm{R}} - \sigma_{\mathrm{L}}^3 \mathbf{d}_{0,\mathrm{R}} \end{bmatrix} \vec{\mathbf{e}}^{\mathsf{T}} + \overline{P}^{-1} \begin{bmatrix} \sigma_{\mathrm{R}}^2 \mathbf{e}_{N,\mathrm{L}} + \sigma_{\mathrm{R}}^4 \mathbf{d}_{N,\mathrm{L}} \\ -\sigma_{\mathrm{L}}^2 \mathbf{e}_{0,\mathrm{R}} - \sigma_{\mathrm{L}}^4 \mathbf{d}_{0,\mathrm{R}} \end{bmatrix} \vec{\mathbf{d}}^{\mathsf{T}},$$

which indeed is a consistent approximation of $\varepsilon\partial^2/\partial x^2$.

3.4 Stability

We multiply the two equations in (8) by $\mathbf{u}_{\mathrm{L}}^{\mathsf{T}} P_{\mathrm{L}}$ and $\mathbf{u}_{\mathrm{R}}^{\mathsf{T}} P_{\mathrm{R}}$, respectively. By adding the results, we obtain the discrete analogue to (2),

$$\begin{aligned} &\frac{\mathrm{d}}{\mathrm{d}t}\left(\mathbf{u}_{\mathrm{L}}^{\mathsf{T}} P_{\mathrm{L}} \mathbf{u}_{\mathrm{L}} + \mathbf{u}_{\mathrm{R}}^{\mathsf{T}} P_{\mathrm{R}} \mathbf{u}_{\mathrm{R}}\right) + 2\varepsilon\left(\mathbf{u}_{\mathrm{L}}^{\mathsf{T}} A_{\mathrm{L}} \mathbf{u}_{\mathrm{L}} + \mathbf{u}_{\mathrm{R}}^{\mathsf{T}} A_{\mathrm{R}} \mathbf{u}_{\mathrm{R}}\right) = \\ &\quad = \begin{bmatrix} \mathbf{e}_{N,\mathrm{L}}^{\mathsf{T}}\mathbf{u}_{\mathrm{L}} + \mathbf{e}_{0,\mathrm{R}}^{\mathsf{T}}\mathbf{u}_{\mathrm{R}} \\ \mathbf{e}_{N,\mathrm{L}}^{\mathsf{T}}\mathbf{u}_{\mathrm{L}} - \mathbf{e}_{0,\mathrm{R}}^{\mathsf{T}}\mathbf{u}_{\mathrm{R}} \\ \mathbf{d}_{N,\mathrm{L}}^{\mathsf{T}}\mathbf{u}_{\mathrm{L}} + \mathbf{d}_{0,\mathrm{R}}^{\mathsf{T}}\mathbf{u}_{\mathrm{R}} \\ \mathbf{d}_{N,\mathrm{L}}^{\mathsf{T}}\mathbf{u}_{\mathrm{L}} - \mathbf{d}_{0,\mathrm{R}}^{\mathsf{T}}\mathbf{u}_{\mathrm{R}} \end{bmatrix}^{\mathsf{T}} \begin{bmatrix} 0 & 0 & 0 & 0 \\ 0 & 2\sigma_{\mathrm{L}}^1 & \varepsilon & \sigma_{\mathrm{L}}^2 + \sigma_{\mathrm{L}}^3 \\ 0 & \varepsilon & 0 & 0 \\ 0 & \sigma_{\mathrm{L}}^2 + \sigma_{\mathrm{L}}^3 & 0 & 2\sigma_{\mathrm{L}}^4 \end{bmatrix} \begin{bmatrix} \mathbf{e}_{N,\mathrm{L}}^{\mathsf{T}}\mathbf{u}_{\mathrm{L}} + \mathbf{e}_{0,\mathrm{R}}^{\mathsf{T}}\mathbf{u}_{\mathrm{R}} \\ \mathbf{e}_{N,\mathrm{L}}^{\mathsf{T}}\mathbf{u}_{\mathrm{L}} - \mathbf{e}_{0,\mathrm{R}}^{\mathsf{T}}\mathbf{u}_{\mathrm{R}} \\ \mathbf{d}_{N,\mathrm{L}}^{\mathsf{T}}\mathbf{u}_{\mathrm{L}} + \mathbf{d}_{0,\mathrm{R}}^{\mathsf{T}}\mathbf{u}_{\mathrm{R}} \\ \mathbf{d}_{N,\mathrm{L}}^{\mathsf{T}}\mathbf{u}_{\mathrm{L}} - \mathbf{d}_{0,\mathrm{R}}^{\mathsf{T}}\mathbf{u}_{\mathrm{R}} \end{bmatrix}, \end{aligned} \tag{12}$$

where we have used the dual consistency demands (11). To show stability, the quadratic form above (containing the interface deviations) must be non-positive. However, the related matrix is indefinite for all $\varepsilon \neq 0$, regardless of the choice of penalty parameters.

To get around this, we use a variant of the technique in [3]. As indicated in (6), let $\mathbf{d}_{N,\mathrm{L}} = S_{\mathrm{L}}^{\mathsf{T}}\mathbf{e}_{N,\mathrm{L}}$, $\mathbf{d}_{0,\mathrm{R}} = S_{\mathrm{R}}^{\mathsf{T}}\mathbf{e}_{0,\mathrm{R}}$ and $A_{\mathrm{L,R}} = S_{\mathrm{L,R}}^{\mathsf{T}} M_{\mathrm{L,R}} S_{\mathrm{L,R}}$. We define the auxiliary variables $\mathbf{w}_{\mathrm{L}} = S_{\mathrm{L}}\mathbf{u}_{\mathrm{L}} - \frac{1}{2}M_{\mathrm{L}}^{-1}\mathbf{e}_{N,\mathrm{L}}(\mathbf{e}_{N,\mathrm{L}}^{\mathsf{T}}\mathbf{u}_{\mathrm{L}} - \mathbf{e}_{0,\mathrm{R}}^{\mathsf{T}}\mathbf{u}_{\mathrm{R}})$ and $\mathbf{w}_{\mathrm{R}} = S_{\mathrm{R}}\mathbf{u}_{\mathrm{R}} - \frac{1}{2}M_{\mathrm{R}}^{-1}\mathbf{e}_{0,\mathrm{R}}(\mathbf{e}_{N,\mathrm{L}}^{\mathsf{T}}\mathbf{u}_{\mathrm{L}} - \mathbf{e}_{0,\mathrm{R}}^{\mathsf{T}}\mathbf{u}_{\mathrm{R}})$ and compute

$$\begin{aligned} \mathbf{w}_{\mathrm{L}}^{\mathsf{T}} M_{\mathrm{L}} \mathbf{w}_{\mathrm{L}} &= \mathbf{u}_{\mathrm{L}}^{\mathsf{T}} A_L \mathbf{u}_{\mathrm{L}} - \mathbf{d}_{N,\mathrm{L}}^{\mathsf{T}}\mathbf{u}_{\mathrm{L}}(\mathbf{e}_{N,\mathrm{L}}^{\mathsf{T}}\mathbf{u}_{\mathrm{L}} - \mathbf{e}_{0,\mathrm{R}}^{\mathsf{T}}\mathbf{u}_{\mathrm{R}}) + \frac{1}{4} q_{\mathrm{L}} (\mathbf{e}_{N,\mathrm{L}}^{\mathsf{T}}\mathbf{u}_{\mathrm{L}} - \mathbf{e}_{0,\mathrm{R}}^{\mathsf{T}}\mathbf{u}_{\mathrm{R}})^2, \\ \mathbf{w}_{\mathrm{R}}^{\mathsf{T}} M_{\mathrm{R}} \mathbf{w}_{\mathrm{R}} &= \mathbf{u}_{\mathrm{R}}^{\mathsf{T}} A_R \mathbf{u}_{\mathrm{R}} - \mathbf{d}_{0,\mathrm{R}}^{\mathsf{T}}\mathbf{u}_{\mathrm{R}}(\mathbf{e}_{N,\mathrm{L}}^{\mathsf{T}}\mathbf{u}_{\mathrm{L}} - \mathbf{e}_{0,\mathrm{R}}^{\mathsf{T}}\mathbf{u}_{\mathrm{R}}) + \frac{1}{4} q_{\mathrm{R}} (\mathbf{e}_{N,\mathrm{L}}^{\mathsf{T}}\mathbf{u}_{\mathrm{L}} - \mathbf{e}_{0,\mathrm{R}}^{\mathsf{T}}\mathbf{u}_{\mathrm{R}})^2, \end{aligned} \tag{13}$$

where $q_{\mathrm{L}} = \mathbf{e}_{N,\mathrm{L}}^{\mathsf{T}} M_{\mathrm{L}}^{-1} \mathbf{e}_{N,\mathrm{L}}$ and $q_{\mathrm{R}} = \mathbf{e}_{0,\mathrm{R}}^{\mathsf{T}} M_{\mathrm{R}}^{-1} \mathbf{e}_{0,\mathrm{R}}$. By replacing the terms $\mathbf{u}_{\mathrm{L}}^{\mathsf{T}} A_{\mathrm{L}} \mathbf{u}_{\mathrm{L}}$ and $\mathbf{u}_{\mathrm{R}}^{\mathsf{T}} A_{\mathrm{R}} \mathbf{u}_{\mathrm{R}}$ in (12) using the relations in (13), we obtain another discrete analogue to (2),

$$\begin{aligned} &\frac{\mathrm{d}}{\mathrm{d}t}\left(\mathbf{u}_{\mathrm{L}}^{\mathsf{T}} P_{\mathrm{L}} \mathbf{u}_{\mathrm{L}} + \mathbf{u}_{\mathrm{R}}^{\mathsf{T}} P_{\mathrm{R}} \mathbf{u}_{\mathrm{R}}\right) + 2\varepsilon\left(\mathbf{w}_{\mathrm{L}}^{\mathsf{T}} M_{\mathrm{L}} \mathbf{w}_{\mathrm{L}} + \mathbf{w}_{\mathrm{R}}^{\mathsf{T}} M_{\mathrm{R}} \mathbf{w}_{\mathrm{R}}\right) = \\ &\quad = \begin{bmatrix} \mathbf{e}_{N,\mathrm{L}}^{\mathsf{T}}\mathbf{u}_{\mathrm{L}} - \mathbf{e}_{0,\mathrm{R}}^{\mathsf{T}}\mathbf{u}_{\mathrm{R}} \\ \mathbf{d}_{N,\mathrm{L}}^{\mathsf{T}}\mathbf{u}_{\mathrm{L}} - \mathbf{d}_{0,\mathrm{R}}^{\mathsf{T}}\mathbf{u}_{\mathrm{R}} \end{bmatrix}^{\mathsf{T}} \begin{bmatrix} 2\left(\sigma_{\mathrm{L}}^1 + \frac{\varepsilon}{4} q_{\mathrm{L}} + \frac{\varepsilon}{4} q_{\mathrm{R}}\right) & \sigma_{\mathrm{L}}^2 + \sigma_{\mathrm{L}}^3 \\ \sigma_{\mathrm{L}}^2 + \sigma_{\mathrm{L}}^3 & 2\sigma_{\mathrm{L}}^4 \end{bmatrix} \begin{bmatrix} \mathbf{e}_{N,\mathrm{L}}^{\mathsf{T}}\mathbf{u}_{\mathrm{L}} - \mathbf{e}_{0,\mathrm{R}}^{\mathsf{T}}\mathbf{u}_{\mathrm{R}} \\ \mathbf{d}_{N,\mathrm{L}}^{\mathsf{T}}\mathbf{u}_{\mathrm{L}} - \mathbf{d}_{0,\mathrm{R}}^{\mathsf{T}}\mathbf{u}_{\mathrm{R}} \end{bmatrix}. \end{aligned}$$

Our particular choice of auxiliary variables $\mathbf{w}_{\mathrm{L}}$ and $\mathbf{w}_{\mathrm{R}}$ has removed the problematic mixed terms in (12). The scheme will be stable (and dual consistent) for all sets of interface penalty parameters having the form

$$\sigma_{\mathrm{L}}^1 = \sigma_{\mathrm{R}}^1 = s_1 - \varepsilon\frac{q_{\mathrm{L}} + q_{\mathrm{R}}}{4}, \quad \begin{matrix} \sigma_{\mathrm{L}}^2 = s_2 + \varepsilon/2 \\ \sigma_{\mathrm{R}}^2 = s_2 - \varepsilon/2 \end{matrix}, \quad \begin{matrix} \sigma_{\mathrm{L}}^3 = s_3 - \varepsilon/2 \\ \sigma_{\mathrm{R}}^3 = s_3 + \varepsilon/2 \end{matrix}, \quad \sigma_{\mathrm{L}}^4 = \sigma_{\mathrm{R}}^4 = s_4, \tag{14}$$

where the parameters $s_{1,2,3,4}$ must fulfill $s_1 \leq 0$, $s_4 \leq 0$ and $(s_2 + s_3)^2 \leq 4 s_1 s_4$.

Remark 3.2. Just as $S_{\mathrm{L,R}}\mathbf{u}_{\mathrm{L,R}}$, the auxiliary variables $\mathbf{w}_{\mathrm{L,R}}$, which have been modified with penalty-like terms, are consistent approximations of u_x in the first and last row.

Remark 3.3. For narrow-stencil second derivative operators, the stability demands on the penalty parameters actually depend on *both* boundaries. Here we have neglected the outer boundaries when defining the auxiliary variables $\mathbf{w}_{\mathrm{L,R}}$, but if they are included in the derivation, it affects $q_{\mathrm{L,R}}$ slightly. This modification (insignificant for fine grids), is accounted for in the q-values tabulated in [3].

4 Transformation into a single-valued interface

Equipped with a stable and dual consistent multi-domain formulation, we now turn to our main task. Using (7) and (14), the scheme (9) can be written

$$\begin{aligned}\frac{\mathrm{d}}{\mathrm{d}t}\vec{\mathbf{u}} = -\varepsilon\overline{P}^{-1}\begin{bmatrix} A_{\mathrm{L}} & 0 \\ 0 & A_{\mathrm{R}} \end{bmatrix}\vec{\mathbf{u}} + \sigma^1_{\mathrm{L,R}}\overline{P}^{-1}\vec{\mathbf{e}}\vec{\mathbf{e}}^{\mathsf{T}}\vec{\mathbf{u}} + \overline{P}^{-1}\begin{bmatrix} (\varepsilon/2+s_2)\mathbf{d}_{N,\mathrm{L}} \\ (\varepsilon/2-s_2)\mathbf{d}_{0,\mathrm{R}} \end{bmatrix}\vec{\mathbf{e}}^{\mathsf{T}}\vec{\mathbf{u}} \\ + \overline{P}^{-1}\vec{\mathbf{e}}\begin{bmatrix} (\varepsilon/2+s_3)\mathbf{d}_{N,\mathrm{L}} \\ (\varepsilon/2-s_3)\mathbf{d}_{0,\mathrm{R}} \end{bmatrix}^{\mathsf{T}}\vec{\mathbf{u}} + s_4\overline{P}^{-1}\vec{\mathbf{d}}\vec{\mathbf{d}}^{\mathsf{T}}\vec{\mathbf{u}}.\end{aligned} \tag{15}$$

Note that both $\mathbf{e}_{N,\mathrm{L}}^{\mathsf{T}}\mathbf{u}_{\mathrm{L}}$ and $\mathbf{e}_{0,\mathrm{R}}^{\mathsf{T}}\mathbf{u}_{\mathrm{R}}$ in $\vec{\mathbf{e}}^{\mathsf{T}}\vec{\mathbf{u}} = \mathbf{e}_{N,\mathrm{L}}^{\mathsf{T}}\mathbf{u}_{\mathrm{L}} - \mathbf{e}_{0,\mathrm{R}}^{\mathsf{T}}\mathbf{u}_{\mathrm{R}} \approx 0$ are approximations of the exact solution value $u(\hat{x},t)$. Our aim is to modify the scheme such that it operates without this double representation at the interface.

4.1 Derivation of the new scheme

We start by defining the matrices $\widetilde{K}$ and $\widetilde{I}$. Their respective purpose is to merge and to duplicate interface values. They are similar to the identity matrix, but their dimensions are $(N+1)\times(N+2)$ and they are modified in the interior: Around row $\hat{\imath}$ and columns $\hat{\imath}$ and $\hat{\imath}+1$ they have the entries

$$\widetilde{K} = \begin{bmatrix} \ddots & & & & & \\ & 1 & 0 & 0 & 0 & \\ & 0 & \alpha & 1-\alpha & 0 & \\ & 0 & 0 & 0 & 1 & \\ & & & & & \ddots \end{bmatrix}, \qquad \widetilde{I} = \begin{bmatrix} \ddots & & & & & \\ & 1 & 0 & 0 & 0 & \\ & 0 & 1 & 1 & 0 & \\ & 0 & 0 & 0 & 1 & \\ & & & & & \ddots \end{bmatrix}, \tag{16}$$

where $\alpha = \mathbf{e}_{N,\mathrm{L}}^{\mathsf{T}}P_{\mathrm{L}}\mathbf{e}_{N,\mathrm{L}}/(\mathbf{e}_{N,\mathrm{L}}^{\mathsf{T}}P_{\mathrm{L}}\mathbf{e}_{N,\mathrm{L}} + \mathbf{e}_{0,\mathrm{R}}^{\mathsf{T}}P_{\mathrm{R}}\mathbf{e}_{0,\mathrm{R}})$. For later reference, we note that

$$\widetilde{I}\begin{bmatrix} c_{\mathrm{L}}\mathbf{e}_{N,\mathrm{L}} \\ c_{\mathrm{R}}\mathbf{e}_{0,\mathrm{R}} \end{bmatrix} = (c_{\mathrm{L}}+c_{\mathrm{R}})\mathbf{e}_{\hat{\imath}}, \quad \mathbf{e}_{\hat{\imath}}^{\mathsf{T}}\widetilde{K} = \begin{bmatrix} \alpha\mathbf{e}_{N,\mathrm{L}} \\ (1-\alpha)\mathbf{e}_{0,\mathrm{R}} \end{bmatrix}^{\mathsf{T}}, \quad \mathbf{e}_{\hat{\imath}} = [0,\ldots,0,1,0,\ldots,0]^{\mathsf{T}}, \tag{17}$$

where $c_{\mathrm{L,R}}$ are arbitrary scalars and $\mathbf{e}_{\hat{\imath}}$ is a $(N+1)\times 1$-vector, non-zero only in row $\hat{\imath}$. In particular, note that $\widetilde{I}\,\vec{\mathbf{e}} = (1-1)\mathbf{e}_{\hat{\imath}} = 0$, where $\vec{\mathbf{e}} = [0,\ldots,0,1,-1,0,\ldots,0]^{\mathsf{T}}$ is given in (10).

Proposition 4.1. *Consider the diagonal matrix $\overline{P}$ in* (10)*. With $\widetilde{K}$ and $\widetilde{I}$ as specified in* (16)*, the relation $\widetilde{K}\overline{P}^{-1} = \widetilde{P}^{-1}\widetilde{I}$ holds, where $\widetilde{P}$ is defined as $\widetilde{P} \equiv \widetilde{I}\,\overline{P}\widetilde{I}^{\mathsf{T}}$.*

Assumption 4.2. $\mathbf{e}_{N,L}^{\mathsf{T}}\mathbf{u}_L \equiv \mathbf{e}_{0,R}^{\mathsf{T}}\mathbf{u}_R$.

Corollary 4.3. *Assumption 4.2 leads to the relation* $\vec{\mathbf{u}} = \widetilde{I}^{\mathsf{T}}\widetilde{K}\vec{\mathbf{u}}$*, where* $\vec{\mathbf{u}}$ *is given in* (10) *and* $\widetilde{K}$ *and* $\widetilde{I}$ *are given in* (16)*.*

Corollary 4.3 and Proposition 4.1 are proven in [4]. For completeness we provide the proofs in A.

We are now ready to derive the new scheme: Since we aim for a single solution value at the interface instead of two, we multiply our original scheme (15) by $\widetilde{K}$ from the left. We thereafter use $\widetilde{K}\overline{P}^{-1} = \widetilde{P}^{-1}\widetilde{I}$ from Proposition 4.1, yielding

$$\widetilde{K}\frac{\mathrm{d}}{\mathrm{d}t}\vec{\mathbf{u}} = -\varepsilon\widetilde{P}^{-1}\widetilde{I}\begin{bmatrix} A_{\mathrm{L}} & 0 \\ 0 & A_{\mathrm{R}} \end{bmatrix}\vec{\mathbf{u}} + \sigma_{\mathrm{L,R}}^1\widetilde{P}^{-1}\widetilde{I}\,\vec{\mathbf{e}}\vec{\mathbf{e}}^{\mathsf{T}}\vec{\mathbf{u}} + \widetilde{P}^{-1}\widetilde{I}\begin{bmatrix} (\varepsilon/2+s_2)\mathbf{d}_{N,\mathrm{L}} \\ (\varepsilon/2-s_2)\mathbf{d}_{0,\mathrm{R}} \end{bmatrix}\vec{\mathbf{e}}^{\mathsf{T}}\vec{\mathbf{u}}$$
$$+ \widetilde{P}^{-1}\widetilde{I}\,\vec{\mathbf{e}}\begin{bmatrix} (\varepsilon/2+s_3)\mathbf{d}_{N,\mathrm{L}} \\ (\varepsilon/2-s_3)\mathbf{d}_{0,\mathrm{R}} \end{bmatrix}^{\mathsf{T}}\vec{\mathbf{u}} + s_4\widetilde{P}^{-1}\widetilde{I}\,\vec{\mathbf{d}}\vec{\mathbf{d}}^{\mathsf{T}}\vec{\mathbf{u}}.$$

Let $\widetilde{K}$ be constant, such that $\widetilde{K}\vec{\mathbf{u}}_t = (\widetilde{K}\vec{\mathbf{u}})_t$ and define $\widetilde{\mathbf{u}} \equiv \widetilde{K}\vec{\mathbf{u}}$. The vector $\widetilde{\mathbf{u}}$ is one element shorter than $\vec{\mathbf{u}}$ and identical to $\vec{\mathbf{u}}$ in all points, except at the interface, where $\mathbf{e}_i^{\mathsf{T}}\widetilde{\mathbf{u}} = \alpha\mathbf{e}_{N,\mathrm{L}}^{\mathsf{T}}\mathbf{u}_{\mathrm{L}} + (1-\alpha)\mathbf{e}_{0,\mathrm{R}}^{\mathsf{T}}\mathbf{u}_{\mathrm{R}}$.

Next, Assumption 4.2 yields $\vec{\mathbf{e}}^{\mathsf{T}}\vec{\mathbf{u}} = \mathbf{e}_{N,\mathrm{L}}^{\mathsf{T}}\mathbf{u}_{\mathrm{L}} - \mathbf{e}_{0,\mathrm{R}}^{\mathsf{T}}\mathbf{u}_{\mathrm{R}} = 0$, which removes the first two penalty terms above. The relation $\widetilde{I}\,\vec{\mathbf{e}} = 0$ from (17) removes the third penalty term. We proceed by replacing $\widetilde{K}\vec{\mathbf{u}}$ by $\widetilde{\mathbf{u}}$ and thereafter, using Corollary 4.3, every remaining $\vec{\mathbf{u}}$ by $\widetilde{I}^{\mathsf{T}}\widetilde{K}\vec{\mathbf{u}} = \widetilde{I}^{\mathsf{T}}\widetilde{\mathbf{u}}$. These steps yield

$$\frac{\mathrm{d}}{\mathrm{d}t}\widetilde{\mathbf{u}} = -\varepsilon\widetilde{P}^{-1}\widetilde{I}\begin{bmatrix} A_{\mathrm{L}} & 0 \\ 0 & A_{\mathrm{R}} \end{bmatrix}\widetilde{I}^{\mathsf{T}}\widetilde{\mathbf{u}} + s_4\widetilde{P}^{-1}\widetilde{I}\,\vec{\mathbf{d}}\vec{\mathbf{d}}^{\mathsf{T}}\widetilde{I}^{\mathsf{T}}\widetilde{\mathbf{u}},$$

with $s_4 \leq 0$ as an optional damping parameter.

If the second order accurate narrow-stencil operator is used in both domains, $s_4 = 0$ will result in the second order stencil in the whole domain, without any special features at the interface. Moreover, numerical experiments suggests that $s_4 \neq 0$ worsens the condition number of the matrix $-\varepsilon\widetilde{P}^{-1}\widetilde{A} + s_4\widetilde{P}^{-1}\widetilde{I}\,\vec{\mathbf{d}}\vec{\mathbf{d}}^{\mathsf{T}}\widetilde{I}^{\mathsf{T}}$, where $\widetilde{A}$ is defined below. This, in addition to simplicity, speaks in favor for $s_4 = 0$. With that choice, our final scheme is

$$\frac{\mathrm{d}}{\mathrm{d}t}\widetilde{\mathbf{u}} = -\varepsilon\widetilde{P}^{-1}\widetilde{A}\widetilde{\mathbf{u}}, \qquad \widetilde{P} = \widetilde{I}\begin{bmatrix} P_{\mathrm{L}} & 0 \\ 0 & P_{\mathrm{R}} \end{bmatrix}\widetilde{I}^{\mathsf{T}}, \qquad \widetilde{A} = \widetilde{I}\begin{bmatrix} A_{\mathrm{L}} & 0 \\ 0 & A_{\mathrm{R}} \end{bmatrix}\widetilde{I}^{\mathsf{T}}. \tag{18}$$

This concludes the derivation. At this point we can forget Assumption 4.2, since (18) is a new scheme, independent of the original one.

5 Properties of the new scheme

In the derivation of the new scheme (18), we rather boldly required that the original solution vector $\vec{\mathbf{u}}$ fulfilled Assumption 4.2, and initially the new solution vector $\widetilde{\mathbf{u}}$ was related to $\vec{\mathbf{u}}$. Below we show that our final scheme (18) is in fact a stand-alone scheme, with the SBP-properties preserved.

5.1 Stability

First, it is easily seen that the scheme is stable, since $\widetilde{P} > 0$ and $\widetilde{A} \geq 0$. Multiplying (18) from the left by $\widetilde{\mathbf{u}}^{\mathsf{T}}\widetilde{P}$, we directly obtain the energy decay

$$\frac{\mathrm{d}}{\mathrm{d}t}\left(\widetilde{\mathbf{u}}^{\mathsf{T}}\widetilde{P}\widetilde{\mathbf{u}}\right) + 2\varepsilon\widetilde{\mathbf{u}}^{\mathsf{T}}\widetilde{A}\widetilde{\mathbf{u}} = 0.$$

Exploiting that $\widetilde{I}^{\mathsf{T}}\widetilde{\mathbf{u}} = [\widetilde{\mathbf{u}}_{\mathrm{L}}^{\mathsf{T}}, \widetilde{\mathbf{u}}_{\mathrm{R}}^{\mathsf{T}}]^{\mathsf{T}}$, where $\widetilde{\mathbf{u}}_{\mathrm{L}}$ refers to the left part of $\widetilde{\mathbf{u}}$ (including the interface value $\mathbf{e}_i^{\mathsf{T}}\widetilde{\mathbf{u}}$) and $\widetilde{\mathbf{u}}_{\mathrm{R}}$ refers to the right part of $\widetilde{\mathbf{u}}$ (also including $\mathbf{e}_i^{\mathsf{T}}\widetilde{\mathbf{u}}$), we can rewrite the above growth rate in an equivalent form, as

$$\frac{\mathrm{d}}{\mathrm{d}t}\left(\widetilde{\mathbf{u}}_{\mathrm{L}}^{\mathsf{T}}P_{\mathrm{L}}\widetilde{\mathbf{u}}_{\mathrm{L}} + \widetilde{\mathbf{u}}_{\mathrm{R}}^{\mathsf{T}}P_{\mathrm{R}}\widetilde{\mathbf{u}}_{\mathrm{R}}\right) + 2\varepsilon\left(\widetilde{\mathbf{u}}_{\mathrm{L}}^{\mathsf{T}}A_{\mathrm{L}}\widetilde{\mathbf{u}}_{\mathrm{L}} + \widetilde{\mathbf{u}}_{\mathrm{R}}^{\mathsf{T}}A_{\mathrm{R}}\widetilde{\mathbf{u}}_{\mathrm{R}}\right) = 0,$$

which more clearly resembles (2). Recall that we omit the contribution from the outer boundaries.

5.2 Accuracy

Next, we show that the new scheme is accurate. Using (5), Proposition 4.1 and (17), the scheme (18) can be rewritten as

$$\frac{\mathrm{d}}{\mathrm{d}t}\widetilde{\mathbf{u}} = \varepsilon\widetilde{K}\begin{bmatrix} D_{2,\mathrm{L}}\widetilde{\mathbf{u}}_{\mathrm{L}} \\ D_{2,\mathrm{R}}\widetilde{\mathbf{u}}_{\mathrm{R}} \end{bmatrix} - \varepsilon\widetilde{P}^{-1}\mathbf{e}_i(\mathbf{d}_{N,\mathrm{L}}^{\mathsf{T}}\widetilde{\mathbf{u}}_{\mathrm{L}} - \mathbf{d}_{0,\mathrm{R}}^{\mathsf{T}}\widetilde{\mathbf{u}}_{\mathrm{R}}). \tag{19}$$

Evaluating (19) point-wise, we obtain

$$\frac{\mathrm{d}}{\mathrm{d}t}(\mathbf{e}_i^{\mathsf{T}}\widetilde{\mathbf{u}}) = \varepsilon\big(\alpha(D_{2,\mathrm{L}}\widetilde{\mathbf{u}}_{\mathrm{L}})_{N_{\mathrm{L}}} + (1-\alpha)(D_{2,\mathrm{R}}\widetilde{\mathbf{u}}_{\mathrm{R}})_0\big) - \varepsilon\mathbf{e}_i^{\mathsf{T}}\widetilde{P}^{-1}\mathbf{e}_i(\mathbf{d}_{N,\mathrm{L}}^{\mathsf{T}}\widetilde{\mathbf{u}}_{\mathrm{L}} - \mathbf{d}_{0,\mathrm{R}}^{\mathsf{T}}\widetilde{\mathbf{u}}_{\mathrm{R}})$$

at the interface and

$$\frac{\mathrm{d}}{\mathrm{d}t}(\mathbf{e}_j^{\mathsf{T}}\widetilde{\mathbf{u}}) = \begin{cases} \varepsilon(D_{2,\mathrm{L}}\widetilde{\mathbf{u}}_{\mathrm{L}})_j & 0 \leq j < \hat{\imath} \\ \varepsilon(D_{2,\mathrm{R}}\widetilde{\mathbf{u}}_{\mathrm{R}})_{j-\hat{\imath}}, & \hat{\imath} < j \leq N \end{cases}$$

elsewhere. At the interface, the scheme is hence nothing but two one-sided operators weighted together, plus an in-built internal penalty on the second interface condition.

Let $\underline{u}$, $\underline{u}_{\mathrm{L}}$ and $\underline{u}_{\mathrm{R}}$ denote the exact solution (projected on to the grids in Ω, Ω_{L} and Ω_{R}, respectively). Note that $\mathbf{e}_{N,\mathrm{L}}^{\mathsf{T}}\underline{u}_{\mathrm{L}} = \mathbf{e}_i^{\mathsf{T}}\underline{u} = \mathbf{e}_{0,\mathrm{R}}^{\mathsf{T}}\underline{u}_{\mathrm{R}}$. Inserting $\underline{u}_{\mathrm{L,R}}$ into (8) yields the truncation errors

$$\begin{aligned} T_e^{\mathrm{L}} &= \frac{\mathrm{d}}{\mathrm{d}t}\underline{u}_{\mathrm{L}} - \varepsilon D_{2,\mathrm{L}}\underline{u}_{\mathrm{L}} - P_{\mathrm{L}}^{-1}(\sigma_{\mathrm{L}}^3\mathbf{e}_{N,\mathrm{L}} + \sigma_{\mathrm{L}}^4\mathbf{d}_{N,\mathrm{L}})(\mathbf{d}_{N,\mathrm{L}}^{\mathsf{T}}\underline{u}_{\mathrm{L}} - \mathbf{d}_{0,\mathrm{R}}^{\mathsf{T}}\underline{u}_{\mathrm{R}}), \\ T_e^{\mathrm{R}} &= \frac{\mathrm{d}}{\mathrm{d}t}\underline{u}_{\mathrm{R}} - \varepsilon D_{2,\mathrm{R}}\underline{u}_{\mathrm{R}} - P_{\mathrm{R}}^{-1}(\sigma_{\mathrm{R}}^3\mathbf{e}_{0,\mathrm{R}} + \sigma_{\mathrm{R}}^4\mathbf{d}_{0,\mathrm{R}})(\mathbf{d}_{0,\mathrm{R}}^{\mathsf{T}}\underline{u}_{\mathrm{R}} - \mathbf{d}_{N,\mathrm{L}}^{\mathsf{T}}\underline{u}_{\mathrm{L}}), \end{aligned}$$

and inserting $\underline{u}$ into the new scheme (19) produces the truncation error

$$\widetilde{T}_e = \frac{\mathrm{d}}{\mathrm{d}t}\underline{u} - \varepsilon\widetilde{K}\begin{bmatrix} D_{2,\mathrm{L}}\underline{u}_{\mathrm{L}} \\ D_{2,\mathrm{R}}\underline{u}_{\mathrm{R}} \end{bmatrix} + \varepsilon\widetilde{P}^{-1}\mathbf{e}_i(\mathbf{d}_{N,\mathrm{L}}^{\mathsf{T}}\underline{u}_{\mathrm{L}} - \mathbf{d}_{0,\mathrm{R}}^{\mathsf{T}}\underline{u}_{\mathrm{R}}).$$

With the penalty parameters in (8) chosen according to (14), it can be shown that

$$\widetilde{T}_e = \widetilde{K} \begin{bmatrix} T_e^{\mathrm{L}} \\ T_e^{\mathrm{R}} \end{bmatrix}, \qquad \mathbf{e}_j^{\mathsf{T}} \widetilde{T}_e = \begin{cases} (T_e^{\mathrm{L}})_j & 0 \le j < \hat{\imath} \\ \alpha (T_e^{\mathrm{L}})_{N_{\mathrm{L}}} + (1-\alpha)(T_e^{\mathrm{R}})_0, & j = \hat{\imath} \\ (T_e^{\mathrm{R}})_{j-\hat{\imath}} & \hat{\imath} < j \le N. \end{cases}$$

The truncation errors from the original SAT interface scheme and from the new scheme are thus identical, except at the interface. Just as for the original scheme, the global order of accuracy of the new scheme is the same as that of the operator $D_{2,\mathrm{L}}$ or $D_{2,\mathrm{R}}$ which has the lowest order.

5.3 Dual consistency

Finally, let $\widetilde{L} = -\varepsilon \widetilde{P}^{-1} \widetilde{A}$ denote the linear, spatial operator in (18). Computing its dual operator as $\widetilde{L}^* = \widetilde{P}^{-1} \widetilde{L}^{\mathsf{T}} \widetilde{P}$, we obtain $\widetilde{L}^* = -\varepsilon \widetilde{P}^{-1} \widetilde{A}^{\mathsf{T}} = \widetilde{L}$, where the last equality holds since $\widetilde{A}$ is symmetric. Thus $\widetilde{L}$ is self-adjoint and the scheme (18) is dual consistent (given that the outer boundary conditions are imposed in a dual consistent manner).

6 Numerical simulations

The technique to merge SBP operators was introduced for the first derivative operator in [4]. In order to be able to handle elliptic and parabolic problems without using the first derivative operator twice (with known drawbacks), we have in the present work extended the technique to second derivatives. To investigate the properties of the new operators and to demonstrate that they work in standalone mode as well as together with the first derivative operators, we will consider three different model problems. We start by solving a couple of steady problems to confirm the stated spatial properties of the new operators. Thereafter, we consider a time-dependent problem. Below we present the semi-discrete scheme which (with modifications) will be used for all three problems.

Consider the advection-diffusion equation with Dirichlet boundary conditions,

$$\begin{aligned} u_t + a u_x &= \varepsilon u_{xx} + f, & x &\in (0,1), \\ u &= g_{\mathrm{L}}, & x &= 0, \\ u &= g_{\mathrm{R}}, & x &= 1, \end{aligned} \tag{20}$$

where f, g_{L} and g_{R} are given data. We want to solve (20) using the new scheme

$$\begin{aligned} \mathbf{u}_t + a \widetilde{P}^{-1} \widetilde{Q} \mathbf{u} = {} & \varepsilon \widetilde{P}^{-1} \left(-\widetilde{A} + \mathbf{e}_N \widetilde{\mathbf{d}}_N^{\mathsf{T}} - \mathbf{e}_0 \widetilde{\mathbf{d}}_0^{\mathsf{T}} \right) \mathbf{u} + \mathbf{f} \\ & + \widetilde{P}^{-1} (\mu_0 \mathbf{e}_0 + \nu_0 \widetilde{\mathbf{d}}_0)(\mathbf{e}_0^{\mathsf{T}} \mathbf{u} - g_{\mathrm{L}}) \\ & + \widetilde{P}^{-1} (\mu_N \mathbf{e}_N + \nu_N \widetilde{\mathbf{d}}_N)(\mathbf{e}_N^{\mathsf{T}} \mathbf{u} - g_{\mathrm{R}}), \end{aligned} \tag{21}$$

where $\mathbf{f}$ is the restriction of f to the grid. $\widetilde{P}$ and $\widetilde{A}$ are given in (18), and the difference matrix $\widetilde{Q} = \widetilde{I}\, \overline{Q}\, \widetilde{I}^{\mathsf{T}}$, with $\overline{Q}$ given below, was derived in [4]. Moreover, since we now

include the outer boundaries, we need $\widetilde{\mathbf{d}}_0 = \widetilde{I}\,\overline{S}^{\mathsf{T}}\widetilde{I}^{\mathsf{T}}\mathbf{e}_0$ and $\widetilde{\mathbf{d}}_N = \widetilde{I}\,\overline{S}^{\mathsf{T}}\widetilde{I}^{\mathsf{T}}\mathbf{e}_N$, with $\overline{S}$ given below (together with $\overline{M}$ which is needed for the penalty parameters). We have

$$\overline{Q} = \begin{bmatrix} Q_{\mathrm{L}} & 0 \\ 0 & Q_{\mathrm{R}} \end{bmatrix}, \qquad \overline{S} = \begin{bmatrix} S_{\mathrm{L}} & 0 \\ 0 & S_{\mathrm{R}} \end{bmatrix}, \qquad \overline{M} = \begin{bmatrix} M_{\mathrm{L}} & 0 \\ 0 & M_{\mathrm{R}} \end{bmatrix}, \tag{22}$$

where $Q_{\mathrm{L,R}}$ are both fulfilling (4) and where $S_{\mathrm{L,R}}$ and $M_{\mathrm{L,R}}$ are associated with $A_{\mathrm{L,R}}$ in $\widetilde{A}$, as specified in (5) and (6). In (21), we use the penalty parameters

$$\begin{aligned} \mu_0 &= -\frac{a+\omega_{\mathrm{L}}}{2} - q_{\mathrm{L}}\varepsilon, \qquad & \nu_0 &= -\varepsilon, \qquad & \omega_{\mathrm{L}} &> 0, \\ \mu_N &= \frac{a-\omega_{\mathrm{R}}}{2} - q_{\mathrm{R}}\varepsilon, \qquad & \nu_N &= \varepsilon, \qquad & \omega_{\mathrm{R}} &> 0, \end{aligned} \tag{23}$$

from [3], which are designed to give a stable and dual consistent numerical solution. For $q_{\mathrm{L}} = \mathbf{e}_0^{\mathsf{T}}\widetilde{I}\,\overline{M}^{-1}\widetilde{I}^{\mathsf{T}}\mathbf{e}_0 = \mathbf{e}_{0,\mathrm{L}}^{\mathsf{T}}M_{\mathrm{L}}^{-1}\mathbf{e}_{0,\mathrm{L}}$ and $q_{\mathrm{R}} = \mathbf{e}_N^{\mathsf{T}}\widetilde{I}\,\overline{M}^{-1}\widetilde{I}^{\mathsf{T}}\mathbf{e}_N = \mathbf{e}_{N,\mathrm{R}}^{\mathsf{T}}M_{\mathrm{R}}^{-1}\mathbf{e}_{N,\mathrm{R}}$, we use the values tabulated in [3]. In B we show that (21) with (23) is stable.

6.1 The Poisson equation

We employ the method of manufactured solutions, and start by solving $-u_{xx} = f(x)$ with Dirichlet boundary conditions, using the steady version of the scheme (21) with $a = 0$ and $\varepsilon = 1$. In this case we use $\omega_{\mathrm{L,R}} = q_{\mathrm{L,R}}$ in (23). In the simulations, we are interested in the discrete L^2-norm of the solution error, i.e. $\|\mathsf{e}\|_{\widetilde{P}}$, where $\mathsf{e} = \mathbf{u} - \underline{u}$ and $\|\mathsf{e}\|_{\widetilde{P}}^2 = \mathsf{e}^{\mathsf{T}}\widetilde{P}\mathsf{e}$. We solve this problem with $f(x) = 30^2\cos(30x)$, such that the exact solution is $u = \cos(30x)$, using schemes that changes order at $\hat{x} = 0.5$. We construct one scheme using wide-stencil operators and one scheme using narrow-stencil operators, and let the left part have interior order 2 and the right part have interior order 6. The resulting solutions and absolute values of the errors are shown in Figure 1(a,c) for the wide-stencil scheme and Figure 1(b,d) for the narrow-stencil scheme, and the corresponding rates of convergence are given in Table 1. As expected, both schemes show a second order convergence rate, which is the lowest order of accuracy of the included operators.

Table 1: Errors and convergence rates corresponding to Figure 1.

N	Wide-stencil operators		Narrow-stencil operators	
	$\|\mathsf{e}\|_{\widetilde{P}}$	$\log_2\left(\frac{\|\mathsf{e}(N/2)\|_{\widetilde{P}}}{\|\mathsf{e}(N)\|_{\widetilde{P}}}\right)$	$\|\mathsf{e}\|_{\widetilde{P}}$	$\log_2\left(\frac{\|\mathsf{e}(N/2)\|_{\widetilde{P}}}{\|\mathsf{e}(N)\|_{\widetilde{P}}}\right)$
32	0.35539437	–	0.23478998	–
64	0.07548625	2.2351	0.06015881	1.9645
128	0.01786133	2.0794	0.01502129	2.0018
256	0.00443970	2.0083	0.00375199	2.0013
512	0.00110933	2.0008	0.00093777	2.0003
1024	0.00027733	2.0000	0.00023443	2.0001

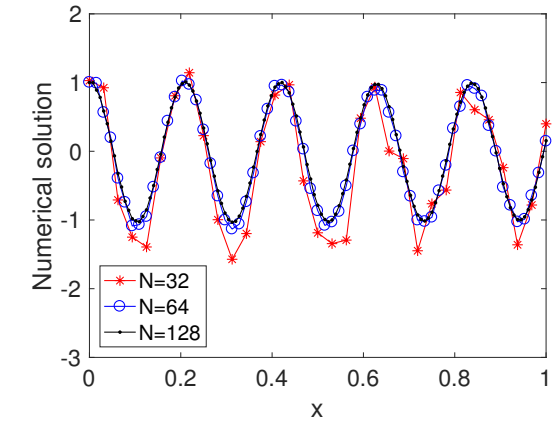

(a) Solutions, wide-stencil operators.

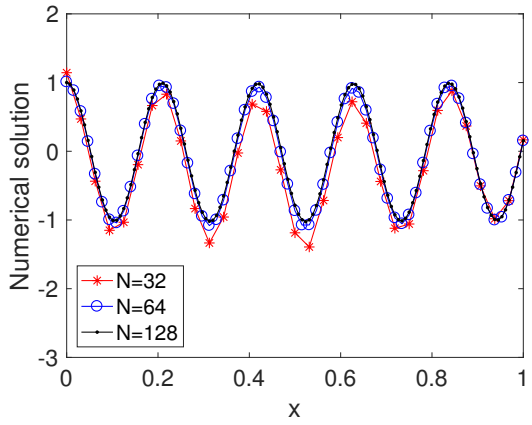

(b) Solutions, narrow-stencil operators.

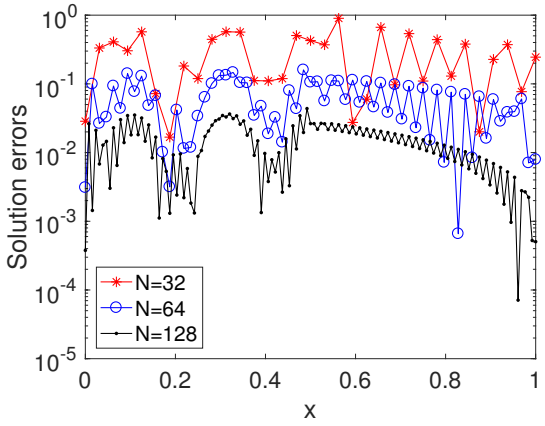

(c) Errors (absolute), wide-stencil operators.

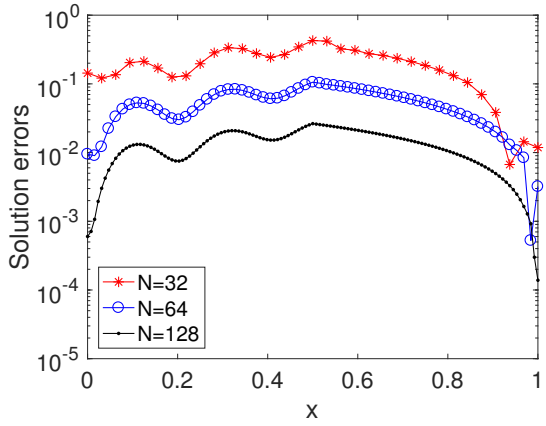

(d) Errors (absolute), narrow-stencil operators.

Figure 1: The schemes have interior order 2 for $x \in [0, 0.5]$ and interior order 6 for $x \in [0.5, 1]$. The exact solution is $u = \cos(30x)$.

6.1.1 Superconvergent functionals

In many applications, functionals are more important than the primary solution itself (e.g. for lift and drag coefficients in computational fluid dynamics). As mentioned, for operators D_1 with interior order of accuracy $2p$ (satisfying (4) with a diagonal P), the accuracy at the boundaries are restricted to order p [9]. Similarly, narrow-stencil operators D_2 with interior order $2p$ and boundary order p (satisfying (5) with a diagonal P) are constructed in [11]. This, in turn, limits the order of accuracy of the resulting L^∞-errors to $p+1$ for the wide-stencil operators and to $p+2$ for the narrow-stencil operators [15, 17]. For more details on accuracy, see also the discussions in [19, 18]. Even so, when the scheme is dual consistent, the output functional can be computed with the full inner order of accuracy $2p$ [8].

We consider linear functionals $\mathcal{J}(u) = \int_\Omega gu \, \mathrm{d}x$, approximated by $J(\mathbf{u}) = \mathbf{g}^\mathsf{T} \widetilde{P} \mathbf{u}$, where $\widetilde{P}$ is the new P-matrix in (18), and in addition to the solution error, we study the functional error $\mathtt{E} = |J(\mathbf{u}) - \mathcal{J}(u)|$. The numerical simulations confirm that the new scheme preserves the superconvergence property. In fact, even when having a wide-

stencil operator in one domain and a narrow-stencil operator (with the same interior order) in the other domain, the functional converges with full order $2p$. This is quite remarkable since the wide- and narrow-stencil operators produce solution errors of different orders. In Figure 2, the resulting errors when using schemes with interior order 6 are shown. The exact solution is $u = \cos(30x)$ and the weight function is $g = \cos(30x)$. In Figure 2(a) we see – again – that the new scheme has the same global order of accuracy as the operator with the lowest order, and in Figure 2(b) the full 6th order convergence rate of the functional is confirmed.

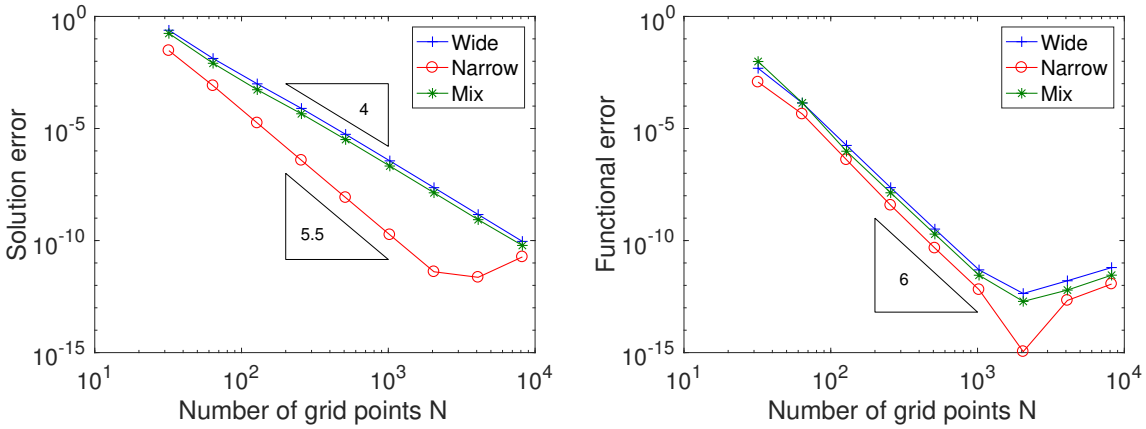

(a) Solution errors $\|\mathsf{e}\|_{\widetilde{P}}$ (b) Functional errors $\mathtt{E}$

Figure 2: The mixed schemes are composed by wide-stencil operators for $x \in [0, 0.5]$ and narrow-stencil operators for $x \in [0.5, 1]$. We use $u(x) = g(x) = \cos(30x)$ and the operators have interior order 6.

6.2 The steady advection-diffusion equation

Next, we consider the steady version of (20). We use $a = 1$, $\varepsilon = 0.01$, $f = 0$, $g_{\mathrm{L}} = 1$ and $g_{\mathrm{R}} = 0$, which leads to an exact solution with a steep gradient at $x = 1$.

To solve this problem, we use the time-independent version of (21), with interior order 2 in the left domain (where the solution is almost flat), and interior order 6 in the right domain (where the boundary layer is located). The penalty parameters μ_0, ν_0, μ_N and ν_N are chosen according to (23), with $\omega_{\mathrm{L,R}} = |a| + \varepsilon q_{\mathrm{L,R}}$ in case of narrow-stencil operators and $\omega_{\mathrm{L,R}} = |a|$ in case of wide-stencil operators (this choice is derived to cancel oscillations [3]).

We first place the interface at $\hat{x} = 0.5$, as before. The resulting numerical solutions and errors can be seen in Figure 3. We see that even though the scheme has higher order of accuracy in the right domain than in the left domain, the magnitude of the errors are clearly largest close to the steep gradient at $x = 1$. The convergence plots that correspond to Figure 3 are shown in Figure 4. Since the main contribution to $\|\mathsf{e}\|_{\widetilde{P}}$ stems from the right part of the domain, there is almost no difference between the new schemes with mixed order and the interface-free schemes with interior order 6.

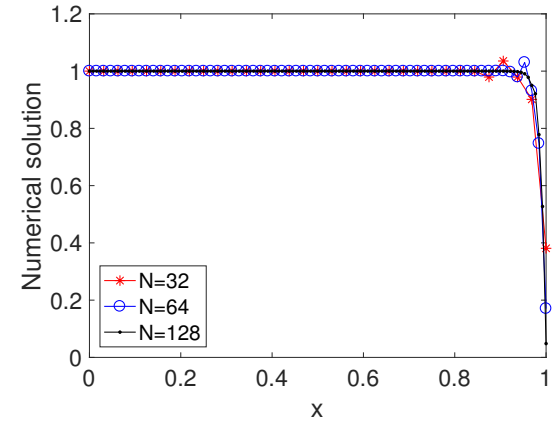

(a) Solutions, wide-stencil operators.

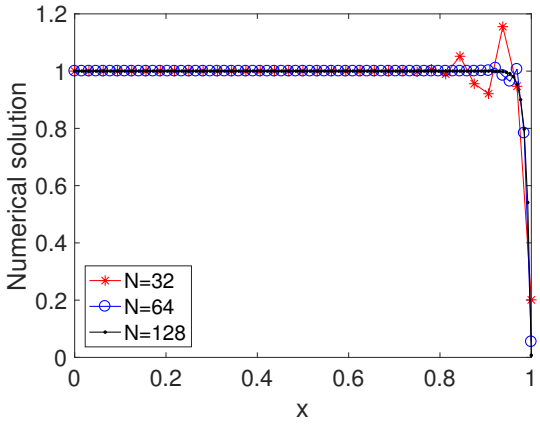

(b) Solutions, narrow-stencil operators.

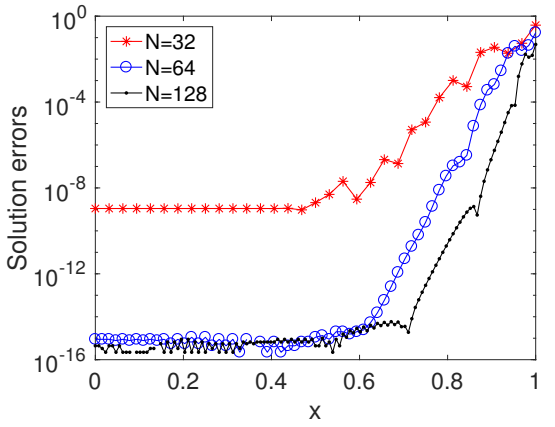

(c) Errors (absolute), wide-stencil operators.

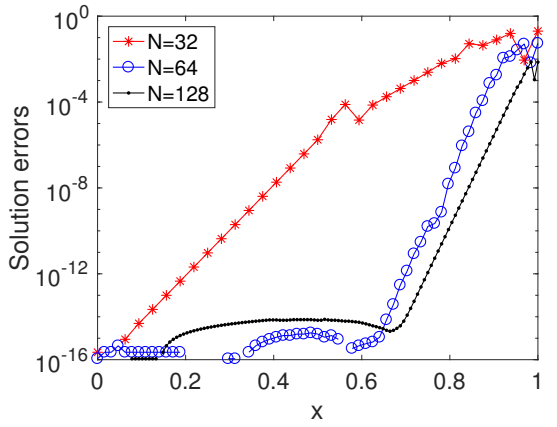

(d) Errors (absolute), narrow-stencil operators.

Figure 3: The schemes have interior order 2 for $x \in [0, 0.5]$ and interior order 6 for $x \in [0.5, 1]$. Exact solution: $u = (e^{ax/\varepsilon} - e^{a/\varepsilon})/(1 - e^{a/\varepsilon})$.

Finally, we place the interface at $\hat{x} = 0.9375$ instead. The standard SBP operators need at least $4p$ grid points, and hence the new scheme under consideration needs $N_{\mathrm{R}} \geq 12$. We thus use $N \geq 192$ when the interface is this close to the boundary. The resulting convergence plots are displayed in Figure 5. Now the second order errors make an impact earlier, and we see that asymptotically, the new schemes converge with second order accuracy, as expected.

Remark 6.1. It is well known that wide-stencil schemes can produce oscillating solutions, but the oscillations decrease as the grid is refined [6]. However, thanks to the particular choice of penalty parameters used here, the interior oscillations are removed completely, as can be seen in Figure 3. In this case the wide-stencil schemes are actually preferable to the narrow-stencil schemes when the resolution is poor, i.e. when $|a|h/\varepsilon$ is large [3].

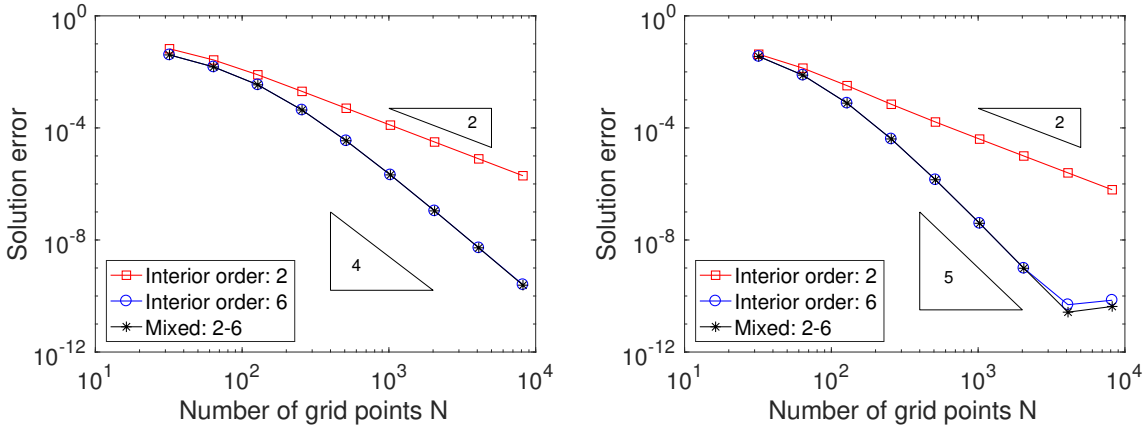

(a) Wide-stencil operators. (b) Narrow-stencil operators.

Figure 4: The errors $\|\mathsf{e}\|_{\widetilde{P}}$ of the mixed scheme when the interface is located at $\hat{x} = 0.5$, compared with schemes without interfaces. The mixed schemes have interior order 2 for $x \in [0, 0.5]$ and interior order 6 for $x \in [0.5, 1]$.

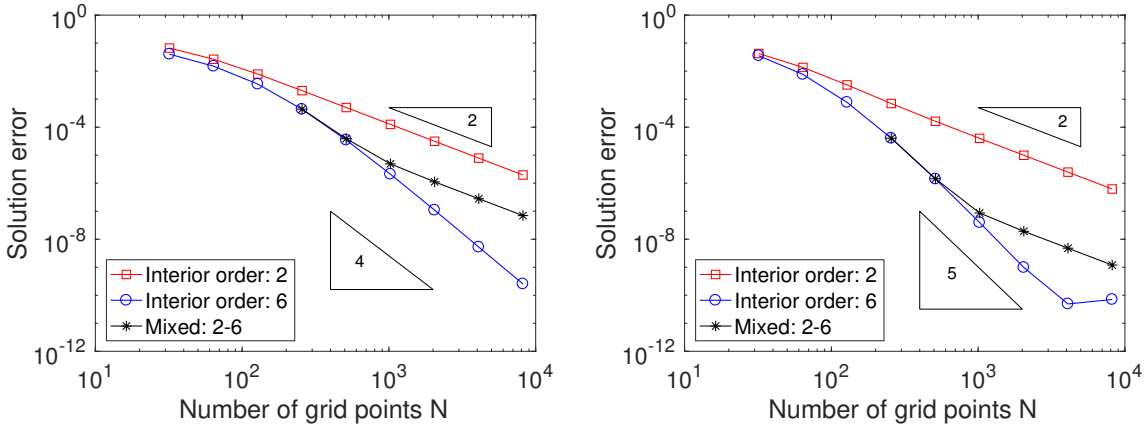

(a) Wide-stencil operators. (b) Narrow-stencil operators.

Figure 5: The errors $\|\mathsf{e}\|_{\widetilde{P}}$ of the mixed scheme when the interface is located in $\hat{x} = 0.9375$, compared with schemes without interfaces. The mixed schemes have interior order 2 for $x \in [0, 0.9375]$ and interior order 6 for $x \in [0.9375, 1]$.

6.3 The unsteady advection-diffusion equation

We now return to the advection-diffusion equation (20). To highlight how the new scheme affects a time-dependent problem, we will follow a Gaussian pulse proceeding through interfaces from one part of the computational domain to the other. With this aim, we let $a = 1$, $\varepsilon = 0.01$, $f(x,t) = 0$, $g_{\mathrm{L}}(t) = e^{-512(t-0.25)^2}$, $g_{\mathrm{R}}(t) = 0$ and $u(x,0) = 0$.

For the spatial discretization, we first use a wide-stencil version of the scheme (21), but with two interfaces; one at $x = 0.25$ and one at $x = 0.5$. In the left and the right part of the domain, the scheme has interior order 6, and between the two interfaces

the scheme is second order accurate. To produce a reference solution, we use a wide-stencil scheme with interior order 6, with the same number of grid points but without interfaces. This choice makes the boundary treatment identical for the two schemes, and allows us to focus on the effect from the lower order accurate region. The penalty parameters are chosen in the same way as in Section 6.2. The semi-discrete schemes are integrated in time using the classical 4th order accurate Runge-Kutta method.

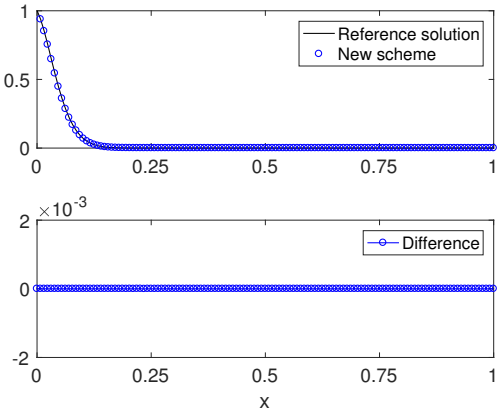

(a) Wide-stencil schemes, time $t = 0.25$

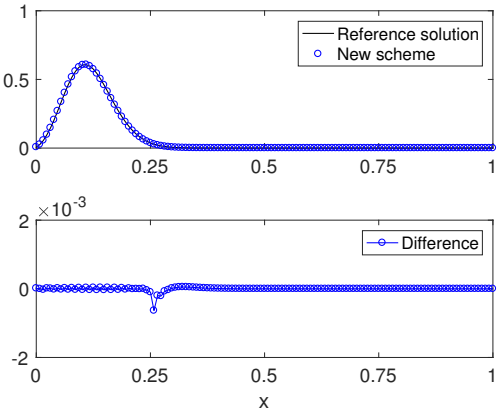

(b) Wide-stencil schemes, time $t = 0.35$

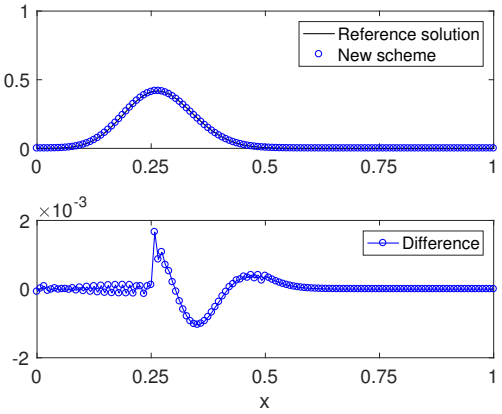

(c) Wide-stencil schemes, time $t = 0.5$

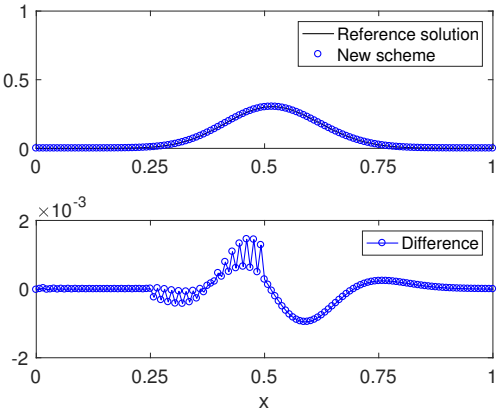

(d) Wide-stencil schemes, time $t = 0.75$

Figure 6: The time evolvement of a Gaussian pulse. The new scheme consists of wide-stencil operators with interior order 6 in the regions $x \in [0, 0.25]$ and $x \in [0.5, 1]$, and order 2 in the region $x \in [0.25, 0.5]$. The reference scheme has interior order 6 and no interfaces.

In Figure 6 we see how the pulse proceeds from one domain to the other. The number of grid points is $N = 128$ and the time step is $\Delta t = 1/25000$ (small enough such that the spatial error dominates).

At time $t = 0.25$, half of the pulse has entered the computational domain, as can be seen in Figure 6(a). Since the new scheme and the reference scheme are identical close to the boundary, the difference between the two numerical solutions is $\sim 10^{-6}$. In Figure 6(b), the pulse has reached the first interface, and now the second order errors become visible. Figure 6(c) shows that the higher order domain $x \in [0, 0.25]$

is relatively unaffected. Since the main propagation direction is from left to right, a significant portion of the lower order errors produced in the region $x \in [0.25, 0.5]$ continue into the higher order accurate region $x \in [0.5, 1]$, as shown in Figure 6(d).

In Figure 7 we show the result for the exact same set-up, but with narrow-stencil second derivative operators D_2 (the reference solution is now produced by a narrow-stencil scheme with interior order 6 and without interfaces). The errors have approximately the same size, but are less oscillatory than in the wide-stencil case.

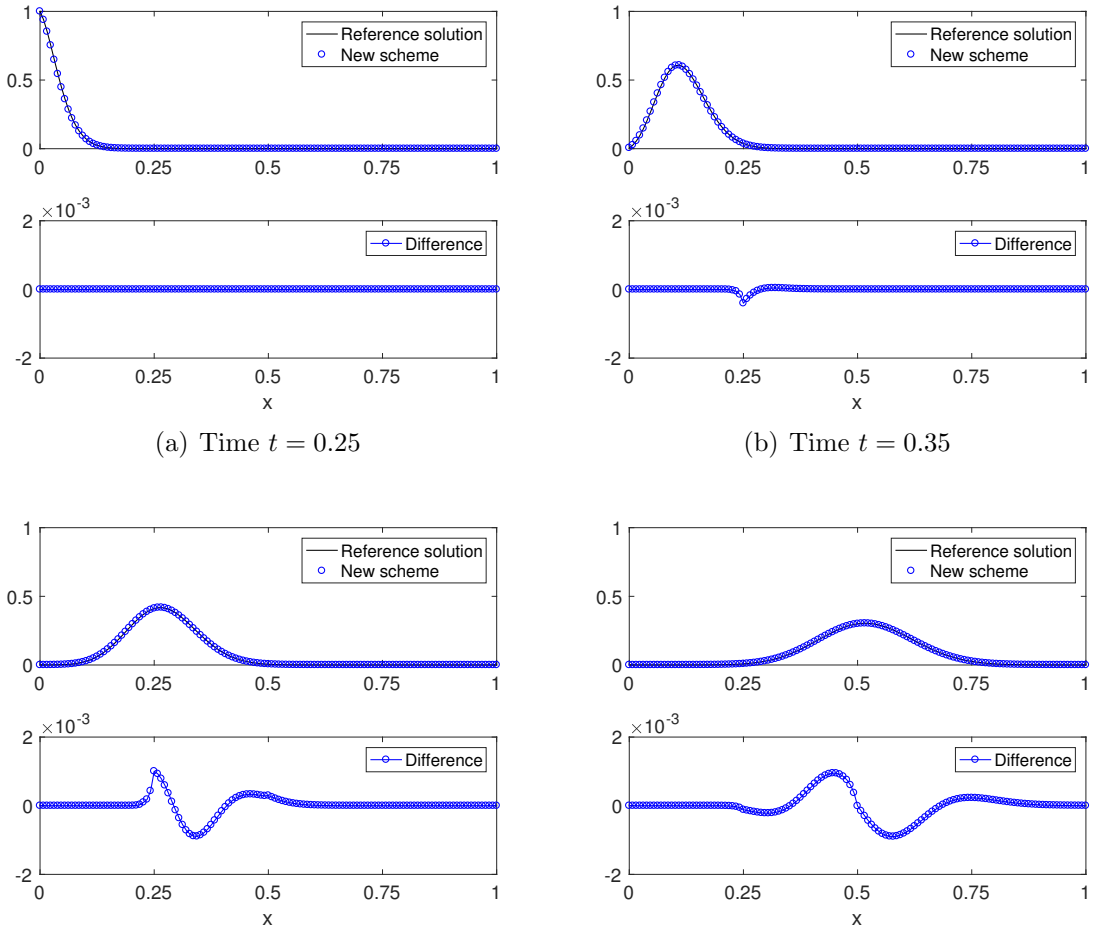

(a) Time $t = 0.25$

(b) Time $t = 0.35$

(c) Time $t = 0.5$

(d) Time $t = 0.75$

Figure 7: The time evolvement of a Gaussian pulse. The new scheme consists of narrow-stencil operators with interior order 6 in the regions $x \in [0, 0.25]$ and $x \in [0.5, 1]$, and order 2 in the region $x \in [0.25, 0.5]$. The reference scheme has interior order 6 and no interfaces.

Figure 8 shows the discrete L^2-norms of the errors (compared to the respective reference solutions). The accuracy of both formulations are similar, and as expected, the overall spatial accuracy is second order.

6.4 Time integration effects

In the above time-dependent simulations, we have used a time-step of $\Delta t = 1/25000$. This step size is not due to accuracy demands but depends on the stability restrictions of

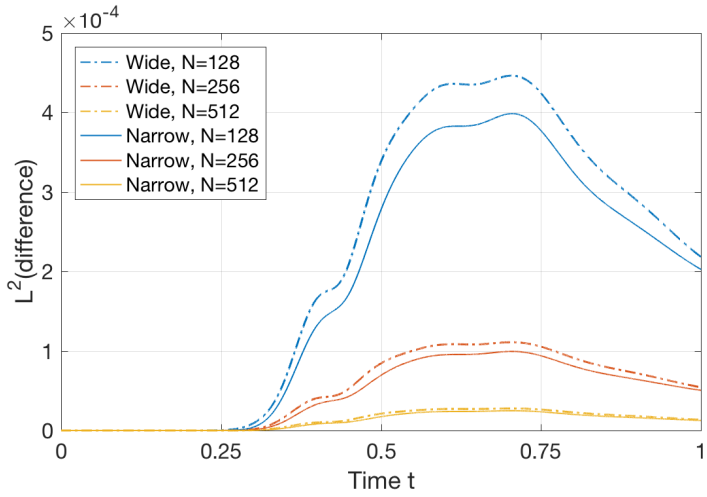

Figure 8: The time evolvement of the errors (compared to more accurate reference solutions).

the Runge-Kutta method. We will investigate these effects, and start by reformulating (21) as $\mathbf{u}_t = \widetilde{L}\mathbf{u} + \widetilde{\mathbf{f}}$, where

$$\widetilde{L} = \widetilde{P}^{-1}\left(-a\widetilde{Q} + \varepsilon\left(-\widetilde{A} + \mathbf{e}_N\widetilde{\mathbf{d}}_N^{\mathsf{T}} - \mathbf{e}_0\widetilde{\mathbf{d}}_0^{\mathsf{T}}\right) + (\mu_0\mathbf{e}_0 + \nu_0\widetilde{\mathbf{d}}_0)\mathbf{e}_0^{\mathsf{T}} + (\mu_N\mathbf{e}_N + \nu_N\widetilde{\mathbf{d}}_N)\mathbf{e}_N^{\mathsf{T}}\right)$$

and where $\widetilde{\mathbf{f}}$ depends on $\mathbf{f}$ and $g_{\mathrm{L,R}}$. The size and location in the complex plane of the eigenvalues (or spectrum) of $\widetilde{L}$, λ_j with $j = 0, 1, \ldots, N$, strongly affect the properties of the numerical scheme. For explicit ODE-solvers, all $z_j = \Delta t\lambda_j$ must lie within the stability region. For the classical 4th order accurate Runge-Kutta method, this means that $\max_j |z_j| \lesssim 2.7$. Thus $\max_j |\lambda_j|$ measures the stiffness of the semi-discrete scheme. Note that the eigenvalues λ_j depend on the penalty parameters (23). The penalty parameters used here give a good compromise between accuracy and stiffness for the original operators [3].

In Table 2 we have listed $\max_j |\lambda_j|$ for the schemes used in the previous section, the reference schemes are denoted "6" and the new schemes "6-2-6". As a comparison we also list the values for the pure second order accurate schemes "2" and a new scheme that have order 2 in the regimes close to the boundaries and interior order 6 between the two interfaces, "2-6-2". First, we note that the pure 6 order schemes are stiffer than the pure 2 order schemes. Secondly (and most importantly), the new schemes are not stiffer than the stiffest included scheme. Finally, somewhat surprisingly, we note that the narrow-stencil based operators are significantly stiffer than the wide-stencil bases ones.

Table 2: The maximum magnitude (rounded) of the eigenvalues of $\widetilde{L}$, that is $\max_j |\lambda_j|$.

	Wide-stencil operators				Narrow-stencil operators			
N	6	6-2-6	2-6-2	2	6	6-2-6	2-6-2	2
128	1001	1001	612	394	3655	3655	2276	858
256	3937	3937	2466	1462	14374	14374	9170	3322
512	15477	15477	11067	5572	57011	57011	36748	13042

7 Summary

A procedure to locally change the type of finite difference stencils in a numerical scheme is developed. The development concerns operators approximating the second derivative, which complements work done earlier for the first derivative. The procedure is useful when the order of a numerical scheme has to be lowered or raised in a specific region of the computational domain.

The new operators are based on summation-by-parts operators with simultaneous approximation term interfaces, but modified such that the numerical solutions have a unique representation in all grid points. This facilitates the process of transferring the interface, which could be especially advantageous for time-dependent problems.

The transition from one type of stencil to another is done in a time-stable and dual consistent manner, and the resulting operators have the same overall accuracy as the lowest included summation-by-parts operator. These properties are verified in numerical experiments on the Poisson equation, the steady advection-diffusion equation and the unsteady advection-diffusion equation. Moreover, in the experiments we note that the new schemes are not stiffer than the stiffest included operator.

A Proofs of Proposition 4.1 and Corollary 4.3

Proof of Proposition 4.1. Consider $\overline{P}$, which is given in (10), $\widetilde{K}$ and $\widetilde{I}$ from (16) and $\widetilde{P} \equiv \widetilde{I}\,\overline{P}\,\widetilde{I}^{\mathsf{T}}$. With $\alpha = \mathbf{e}_{N,\mathrm{L}}^{\mathsf{T}} P_{\mathrm{L}} \mathbf{e}_{N,\mathrm{L}} / (\mathbf{e}_{N,\mathrm{L}}^{\mathsf{T}} P_{\mathrm{L}} \mathbf{e}_{N,\mathrm{L}} + \mathbf{e}_{0,\mathrm{R}}^{\mathsf{T}} P_{\mathrm{R}} \mathbf{e}_{0,\mathrm{R}})$ inserted into $\widetilde{K}$, we have

$$
\begin{aligned}
\widetilde{P}\widetilde{K} &= \begin{bmatrix} \ddots & & & & & \\ & P_{\mathrm{L}}^{N_{\mathrm{L}}-1} & & & & \\ & & P_{\mathrm{L}}^{N_{\mathrm{L}}} + P_{\mathrm{R}}^{0} & & & \\ & & & P_{\mathrm{R}}^{1} & & \\ & & & & \ddots & \end{bmatrix} \begin{bmatrix} \ddots & & & & \\ & 1 & 0 & 0 & \\ & 0 & \frac{P_{\mathrm{L}}^{N_{\mathrm{L}}}}{P_{\mathrm{L}}^{N_{\mathrm{L}}}+P_{\mathrm{R}}^{0}} & \frac{P_{\mathrm{R}}^{0}}{P_{\mathrm{L}}^{N_{\mathrm{L}}}+P_{\mathrm{R}}^{0}} & 0 & \\ & 0 & 0 & 0 & 1 & \\ & & & & & \ddots \end{bmatrix} \\
&= \begin{bmatrix} \ddots & & & & \\ & P_{\mathrm{L}}^{N_{\mathrm{L}}-1} & 0 & 0 & 0 \\ & 0 & P_{\mathrm{L}}^{N_{\mathrm{L}}} & P_{\mathrm{R}}^{0} & 0 \\ & 0 & 0 & 0 & P_{\mathrm{R}}^{1} \\ & & & & \ddots \end{bmatrix} \\
&= \begin{bmatrix} \ddots & & & & \\ & 1 & 0 & 0 & 0 \\ & 0 & 1 & 1 & 0 \\ & 0 & 0 & 0 & 1 \\ & & & & \ddots \end{bmatrix} \begin{bmatrix} \ddots & & & & & \\ & P_{\mathrm{L}}^{N_{\mathrm{L}}-1} & & & & \\ & & P_{\mathrm{L}}^{N_{\mathrm{L}}} & & & \\ & & & P_{\mathrm{R}}^{0} & & \\ & & & & P_{\mathrm{R}}^{1} & \\ & & & & & \ddots \end{bmatrix} = \widetilde{I}\,\overline{P},
\end{aligned}
$$

where P_{L}^{j} and P_{R}^{j} refer to the j^{th} diagonal entry of P_{L} or P_{R}, respectively. Having shown that $\widetilde{P}\widetilde{K} = \widetilde{I}\,\overline{P}$ for diagonal matrices $\overline{P}$, the relation $\widetilde{K}\overline{P}^{-1} = \widetilde{P}^{-1}\widetilde{I}$ follows. □

Proof of Corollary 4.3. From the definitions of $\widetilde{K}$ and $\widetilde{I}$, given in (16), and $\vec{\mathbf{u}}$, which is given in (10), we compute

$$\widetilde{I}^{\mathsf{T}}\widetilde{K}\vec{\mathbf{u}} = \begin{bmatrix} \ddots & & & & & \\ & 1 & 0 & 0 & 0 & \\ & 0 & \alpha & 1-\alpha & 0 & \\ & 0 & \alpha & 1-\alpha & 0 & \\ & 0 & 0 & 0 & 1 & \\ & & & & & \ddots \end{bmatrix} \begin{bmatrix} \vdots \\ (\mathbf{u}_{\mathrm{L}})_{N_{\mathrm{L}}-1} \\ (\mathbf{u}_{\mathrm{L}})_{N_{\mathrm{L}}} \\ (\mathbf{u}_{\mathrm{R}})_0 \\ (\mathbf{u}_{\mathrm{R}})_1 \\ \vdots \end{bmatrix} = \begin{bmatrix} \vdots \\ (\mathbf{u}_{\mathrm{L}})_{N_{\mathrm{L}}-1} \\ \alpha(\mathbf{u}_{\mathrm{L}})_{N_{\mathrm{L}}} + (1-\alpha)(\mathbf{u}_{\mathrm{R}})_0 \\ \alpha(\mathbf{u}_{\mathrm{L}})_{N_{\mathrm{L}}} + (1-\alpha)(\mathbf{u}_{\mathrm{R}})_0 \\ (\mathbf{u}_{\mathrm{R}})_1 \\ \vdots \end{bmatrix}.$$

Assumption 4.2, that is that $(\mathbf{u}_{\mathrm{L}})_{N_{\mathrm{L}}} = (\mathbf{u}_{\mathrm{R}})_0$, leads to $\alpha(\mathbf{u}_{\mathrm{L}})_{N_{\mathrm{L}}} + (1-\alpha)(\mathbf{u}_{\mathrm{R}})_0 = (\mathbf{u}_{\mathrm{L}})_{N_{\mathrm{L}}}$ and $\alpha(\mathbf{u}_{\mathrm{L}})_{N_{\mathrm{L}}} + (1-\alpha)(\mathbf{u}_{\mathrm{R}})_0 = (\mathbf{u}_{\mathrm{R}})_0$. Thus $\vec{\mathbf{u}} = \widetilde{I}^{\mathsf{T}}\widetilde{K}\vec{\mathbf{u}}$ holds. □

B Stability of the advection-diffusion scheme

We multiply the scheme (21) (for simplicity with $\mathbf{f} = 0$ and $g_{\mathrm{L,R}} = 0$) by $\mathbf{u}^{\mathsf{T}}\widetilde{P}$ from the left, and add the transpose. Thereafter using that $\widetilde{Q} + \widetilde{Q}^{\mathsf{T}} = \mathbf{e}_N\mathbf{e}_N^{\mathsf{T}} - \mathbf{e}_0\mathbf{e}_0^{\mathsf{T}}$, yields

$$\begin{aligned} \frac{\mathrm{d}}{\mathrm{d}t}(\mathbf{u}^{\mathsf{T}}\widetilde{P}\mathbf{u}) + 2\varepsilon\mathbf{u}^{\mathsf{T}}\widetilde{A}\mathbf{u} = a\mathbf{u}^{\mathsf{T}}\mathbf{e}_0\mathbf{e}_0^{\mathsf{T}}\mathbf{u} - 2\varepsilon\mathbf{u}^{\mathsf{T}}\mathbf{e}_0\widetilde{\mathbf{d}}_0^{\mathsf{T}}\mathbf{u} + 2\mathbf{u}^{\mathsf{T}}(\mu_0\mathbf{e}_0 + \nu_0\widetilde{\mathbf{d}}_0)\mathbf{e}_0^{\mathsf{T}}\mathbf{u} \\ - a\mathbf{u}^{\mathsf{T}}\mathbf{e}_N\mathbf{e}_N^{\mathsf{T}}\mathbf{u} + 2\varepsilon\mathbf{u}^{\mathsf{T}}\mathbf{e}_N\widetilde{\mathbf{d}}_N^{\mathsf{T}}\mathbf{u} + 2\mathbf{u}^{\mathsf{T}}(\mu_N\mathbf{e}_N + \nu_N\widetilde{\mathbf{d}}_N)\mathbf{e}_N^{\mathsf{T}}\mathbf{u}. \end{aligned} \tag{24}$$

Next, we define $\widetilde{\mathbf{w}} = \overline{S}\,\widetilde{I}^{\mathsf{T}}\mathbf{u} + \overline{M}^{-1}\widetilde{I}^{\mathsf{T}}\mathbf{e}_0\mathbf{e}_0^{\mathsf{T}}\mathbf{u} - \overline{M}^{-1}\widetilde{I}^{\mathsf{T}}\mathbf{e}_N\mathbf{e}_N^{\mathsf{T}}\mathbf{u}$, with $\overline{S}$ and $\overline{M}$ given in (22), and compute

$$\widetilde{\mathbf{w}}^{\mathsf{T}}\overline{M}\,\widetilde{\mathbf{w}} = \mathbf{u}^{\mathsf{T}}\widetilde{A}\mathbf{u} + 2\widetilde{\mathbf{d}}_0^{\mathsf{T}}\mathbf{u}\mathbf{e}_0^{\mathsf{T}}\mathbf{u} - 2\widetilde{\mathbf{d}}_N^{\mathsf{T}}\mathbf{u}\mathbf{e}_N^{\mathsf{T}}\mathbf{u} + q_{\mathrm{L}}(\mathbf{e}_0^{\mathsf{T}}\mathbf{u})^2 + q_{\mathrm{R}}(\mathbf{e}_N^{\mathsf{T}}\mathbf{u})^2, \tag{25}$$

where we have exploited that

$$\begin{aligned} \mathbf{e}_0^{\mathsf{T}}\widetilde{I}\,\overline{M}^{-1}\widetilde{I}^{\mathsf{T}}\mathbf{e}_0 &= \mathbf{e}_{0,\mathrm{L}}^{\mathsf{T}}M_{\mathrm{L}}^{-1}\mathbf{e}_{0,\mathrm{L}} \equiv q_{\mathrm{L}}, & \mathbf{e}_N^{\mathsf{T}}\widetilde{I}\,\overline{M}^{-1}\widetilde{I}^{\mathsf{T}}\mathbf{e}_0 &= 0, \\ \mathbf{e}_N^{\mathsf{T}}\widetilde{I}\,\overline{M}^{-1}\widetilde{I}^{\mathsf{T}}\mathbf{e}_N &= \mathbf{e}_{N,\mathrm{R}}^{\mathsf{T}}M_{\mathrm{R}}^{-1}\mathbf{e}_{N,\mathrm{R}} \equiv q_{\mathrm{R}}, & \mathbf{e}_0^{\mathsf{T}}\widetilde{I}\,\overline{M}^{-1}\widetilde{I}^{\mathsf{T}}\mathbf{e}_N &= 0. \end{aligned}$$

Using (25) in (24) leads to the energy growth rate

$$\frac{\mathrm{d}}{\mathrm{d}t}(\mathbf{u}^{\mathsf{T}}\widetilde{P}\mathbf{u}) + 2\varepsilon\widetilde{\mathbf{w}}^{\mathsf{T}}\overline{M}\,\widetilde{\mathbf{w}} = -\omega_{\mathrm{L}}(\mathbf{e}_0^{\mathsf{T}}\mathbf{u})^2 - \omega_{\mathrm{R}}(\mathbf{e}_N^{\mathsf{T}}\mathbf{u})^2 \leq 0,$$

where we have also used the choice of penalty parameters suggested in (23).

Remark B.1. In contrast to what is generally the case when using narrow-stencil second derivative operators, the modification of $q_{\mathrm{L,R}}$ mentioned in Remark 3.3 is not needed. This is because $\overline{M}$ is block-diagonal, which leads to $\mathbf{e}_N^{\mathsf{T}}\widetilde{I}\,\overline{M}^{-1}\widetilde{I}^{\mathsf{T}}\mathbf{e}_0 = \mathbf{e}_0^{\mathsf{T}}\widetilde{I}\,\overline{M}^{-1}\widetilde{I}^{\mathsf{T}}\mathbf{e}_N = 0$.

References

[1] J. Berg and J. Nordström. On the impact of boundary conditions on dual consistent finite difference discretizations. *Journal of Computational Physics*, 236:41–55, 2013.

[2] M. H Carpenter, J. Nordström, and D. Gottlieb. A stable and conservative interface treatment of arbitrary spatial accuracy. *Journal of Computational Physics*, 148(2):341–365, 1999.

[3] S. Eriksson. A dual consistent finite difference method with narrow stencil second derivative operators. *Journal of Scientific Computing*, 75(2):906–940, 2018.

[4] S. Eriksson, Q. Abbas, and J. Nordström. A stable and conservative method for locally adapting the design order of finite difference schemes. *Journal of Computational Physics*, 230(11):4216–4231, 2011.

[5] D. C. Del Rey Fernández, J. E. Hicken, and D. W. Zingg. Review of summation-by-parts operators with simultaneous approximation terms for the numerical solution of partial differential equations. *Computers & Fluids*, 95:171–196, 2014.

[6] H. Frenander and J. Nordström. Spurious solutions for the advection-diffusion equation using wide stencils for approximating the second derivative. *Numerical Methods for Partial Differential Equations*, 34(2):501–517, 2018.

[7] B. Gustafsson, H.-O. Kreiss, and J. Oliger. *Time-Dependent Problems and Difference Methods*. John Wiley & Sons, Inc., 2013.

[8] J. E. Hicken and D. W. Zingg. Superconvergent functional estimates from summation-by-parts finite-difference discretizations. *SIAM Journal on Scientific Computing*, 33(2):893–922, 2011.

[9] H.-O. Kreiss and G. Scherer. *Finite element and finite difference methods for hyperbolic partial differential equations, in: Mathematical Aspects of Finite Elements in Partial Differential Equations*. Academic Press, Inc., 1974.

[10] V. Linders, T. Lundquist, and J. Nordström. On the order of accuracy of finite difference operators on diagonal norm based summation-by-parts form. *SIAM Journal on Numerical Analysis*, 56(2):1048–1063, 2018.

[11] K. Mattsson and J. Nordström. Summation by parts operators for finite difference approximations of second derivatives. *Journal of Computational Physics*, 199(2):503–540, 2004.

[12] J. Nordström, J. Gong, E. van der Weide, and M. Svärd. A stable and conservative high order multi-block method for the compressible Navier-Stokes equations. *Journal of Computational Physics*, 228(24):9020–9035, 2009.

[13] J. Nordström and M. Svärd. Well-posed boundary conditions for the Navier-Stokes equations. *SIAM Journal on Numerical Analysis*, 43(3):1231–1255, 2005.

[14] B. Strand. Summation by parts for finite difference approximation for d/dx. *Journal of Computational Physics*, 110(1):47 – 67, 1994.

[15] M. Svärd and J. Nordström. On the order of accuracy for difference approximations of initial-boundary value problems. *Journal of Computational Physics*, 218(1):333–352, 2006.

[16] M. Svärd and J. Nordström. Review of summation-by-parts schemes for initial-boundary-value problems. *Journal of Computational Physics*, 268:17–38, 2014.

[17] M. Svärd and J. Nordström. On the convergence rates of energy-stable finite-difference schemes. Technical Report LiTH-MAT-R–2017/14–SE, Linköping University, Department of Mathematics, 2017.

[18] M. Svärd and J. Nordström. Response to "Convergence of summation-by-parts finite difference methods for the wave equation". *Journal of Scientific Computing*, 74(2):1188–1192, 2018.

[19] S. Wang and G. Kreiss. Convergence of summation-by-parts finite difference methods for the wave equation. *Journal of Scientific Computing*, 71(1):219–245, 2017.